DESIGN AND PRELIMINARY FINITE ELEMENT ANALYSIS OF PLANAR ROTARY SPRING FOR BIOAPPS ROMICP® ANKLE-FOOT PROSTHESIS

AUFAR SYEHAN

FACULTY OF ENGINEERING
UNIVERSITY OF MALAYA
KUALA LUMPUR

2022

DESIGN AND PRELIMINARY FINITE ELEMENT ANALYSIS OF PLANAR ROTARY SPRING FOR BIOAPPS ROMICP® ANKLE-FOOT PROSTHESIS

AUFAR SYEHAN

THESIS SUBMITTED IN PARTIAL FULFILMENT OF THE REQUIREMENTS FOR THE MASTER OF BIOMEDICAL ENGINEERING

**FACULTY OF ENGINEERING
UNIVERSITY OF MALAYA
KUALA LUMPUR**

2022

UNIVERSITY OF MALAYA

ORIGINAL LITERARY WORK DECLARATION

Name of Candidate: Aufar Syehan

Matric No: S2019565

Name of Degree: Master of Biomedical Engineering

Title of Project Paper/Research Report/Dissertation/Thesis ("this Work"): Design and Preliminary Finite Element Analysis of Planar Rotary Spring for BioApps RoMicP® Ankle-Foot Prosthesis

Field of Study: Biomechanics, Mechanical Design

I do solemnly and sincerely declare that:

(1) I am the sole author/writer of this Work;
(2) This Work is original;
(3) Any use of any work in which copyright exists was done by way of fair dealing and for permitted purposes and any excerpt or extract from, or reference to or reproduction of any copyright work has been disclosed expressly and sufficiently and the title of the Work and its authorship have been acknowledged in this Work;
(4) I do not have any actual knowledge nor do I ought reasonably to know that the making of this work constitutes an infringement of any copyright work;
(5) I hereby assign all and every rights in the copyright to this Work to the University of Malaya ("UM"), who henceforth shall be owner of the copyright in this Work and that any reproduction or use in any form or by any means whatsoever is prohibited without the written consent of UM having been first had and obtained;
(6) I am fully aware that if in the course of making this Work I have infringed any copyright whether intentionally or otherwise, I may be subject to legal action or any other action as may be determined by UM.

Candidate's Signature Date: 9 February 2022

Subscribed and solemnly declared before,

Witness's Signature Date: 1/3/2022

Name: Dr Nooranida Arifin

Designation: Senior Lecturer
Department of Biomedical Engineering
Faculty of Engineering
University of Malaya
50603 Kuala Lumpur

DESIGN AND PRELIMINARY FINITE ELEMENT ANALYSIS OF PLANAR ROTARY SPRING FOR BIOAPPS ROMICP® ANKLE-FOOT PROSTHESIS

ABSTRACT

Series elastic actuator (SEA) is an excellent option for a powered ankle-foot prosthesis. However, to achieve the best actuator performance, the optimum stiffness of the planar rotary spring should be defined by using a dynamic model. The main objective of this study is to develop a planar rotary spring design with an optimum stiffness. Maraging 300 Alloy Steel or commercially known as Vascomax-300 was selected as the material of the planar rotary spring for the BioApps RoMicP® ankle-foot prosthesis. Furthermore, Archimedean spiral was chosen as the topological shape of the spring.

The spring model was developed in an iterative method, where the width and thickness of the spring' arm were the parameters to be modified until the spring model reached the optimum stiffness value. The definition of an optimum torsional spring stiffness is when the power required by the motor is minimum. Following the completion of the design advancement the reliability of the preliminary spring design was examined by using the Finite Element Method (FEM). Based on the simulation, the planar rotary spring model was able to withstand a maximum torque of 102.793 Nm. The spring rotation was 0.163 rad, corresponding to a torsional stiffness between 620 and 630 Nm/rad.

Keywords: Series elastic actuator, planar rotary spring, torsional stiffness, finite element method.

BENTUK DAN ANALISIS ELEMEN FINITE AWAL PLANAR ROTARY SPRING UNTUK BIOAPPS R0MICP® PERGELANGAN KAKI PROSTESIS

ABSTRAK

Series Elastic Actuator (SEA) merupakan pilihan terbaik untuk prostesis pergelangan berkuasa. Walau bagaimanapun, untuk mencapai prestasi penggerak yang terbaik, kekukuhan optimum planar rotary spring harus ditakrifkan dengan menggunakan model dinamik. Objektif utama kajian ini adalah untuk membangunkan reka bentuk planar rotary spring dengan kekukuhan optimum. Maraging 300 Alloy Steel atau dikenali secara komersial sebagai Vascomax-300 dipilih sebagai bahan planar rotary spring untuk prostesis pergelangan kaki BioApps RoMicP. Tambahan pula, lingkaran Archimedean dipilih sebagai bentuk topologi spring.

Model spring dibangunkan dalam kaedah berulang, di mana lebar dan ketebalan lengan spring akan menjadi parameter untuk diubah suai sehingga model spring mencapai nilai kekukuhan optimum. Takrifan kekakuan spring kilasan optimum ialah apabila kuasa yang diperlukan oleh motor adalah minimum. Setelah proses reka bentuk selesai, kebolehpercayaan reka bentuk spring awal akan diperiksa dengan menggunakan Finite Element Method (FEM). Berdasarkan simulasi, model planar rotary spring mampu menahan tork maksimum 102.793 Nm. Putaran spring ialah sebesar 0.163 rad, sepadan dengan kekukuhan kilasan di antara 620 dan 630 Nm/rad.

Kata kunci: Series elastic actuator, spring rotary planar, kekakuan kilasan, finite element method

ACKNOWLEDGEMENTS

First and foremost, I would like to praise and thank God, the Almighty, for showering the writer with many blessings, knowledge, and opportunities that enabled me to finally complete this final research project.

Apart from my efforts, the success of my thesis is highly dependent on the support and guidance of several individuals. I would want to use this occasion to convey my thanks to everyone who contributed to the successful completion of my thesis. I would like to express my sincerest gratitude towards my supervisor Prof. Ir. Dr. Noor Azuan Abu Osman for his guidance, patience, motivation enthusiasm, and immense knowledge. Moreover, I would like to thank Mr. Jingjing Liu for taking the time to discuss this work and for his assistance and support in completing the objectives of this study.

Last but not least, I would like to thank my family for their countless support given to me during my studies. I am forever indebted to my parents for granting me the priceless opportunities and experiences that have shaped who I am today. They generously encouraged me to pursue new avenues in life and to seek my own destiny. Without them, this journey would not have been possible, and therefore, I dedicate this milestone to them.

TABLE OF CONTENTS

LIST OF FIGURES

LIST OF TABLES

LIST OF SYMBOLS AND ABBREVIATIONS

APDL	:	ANSYS Parametric Design Language
CSEA	:	Compact Series Elastic Actuator
CE	:	Contractile Element
DD	:	Direct Drive
ER	:	Energy Requirements
ESAR	:	Energy Storing and Return Prosthetic
FEA	:	Finite Element Analysis
FEM	:	Finite Element Method
ICF	:	International Classification of Functioning, Impairment, and Health
PEA	:	Parallel Elastic Actuator
PEDA	:	Parallel Elastic Damping Actuator
PE	:	Parallel Elements
PP	:	Peak Power
PPAM	:	Pleated Pneumatic Artificial Muscles
SAFFiR	:	Shipboard Autonomous Firefighting Robot
SEA	:	Series Elastic Actuator
SEDA	:	Series Elastic Damping Actuator
THOR	:	Tactical Hazardous Operations Robot
UPS	:	Unidirectional Parallel Spring
WHO	:	World Health Organization
B_m		The damping coefficient
J_a		The rotational moment of inertia of the ankle
J_m		The rotational moment of inertia of the motor and gearhead
K_s		The torsional stiffness

P_m	The motor's power
θ_a	The ankle's position
θ_m	The motor's position
$\dot{\theta}_a$	The ankle's velocity
$\dot{\theta}_m$	the motor's velocity
$\ddot{\theta}_a$	the ankle's acceleration
$\ddot{\theta}_m$	the motor's acceleration
τ_b	the damping's torque
τ_m	the motor's torque
τ_s	the spring's torque

LIST OF APPENDICES

CHAPTER 1: INTRODUCTION

1.1 Overview

Amputees' stride and everyday routines are profoundly impacted by the loss of a leg. Lower limb amputation, as defined by the International Classification of Functioning, Impairment, and Health (ICF), is a type of physical impairment that affects lower extremity structures and results in gait limitations and participation restrictions (World Health Organization, 2011). In the United States, over 150,000 amputations are perpetrated each year, which equates to 411 persons losing a leg everyday (Molina and Faulk, 2021). Furthermore, over 90% of lower-limb amputations are executed in consequence of vascular disease, with diabetes mellitus accounting for a large part of those individuals (Dillingham et al., 2002). Moreover, According to World Health Organization, 0.5% of the population of a developing country have a disability that will require a prosthesis or orthosis and related rehabilitation services. This prediction suggests that around 160,000 of Malaysia's current population of 32 million need prosthetic or orthotic devices (Arifin et al., 2017).

After amputations are performed, one of the rehabilitation goals is to recover amputees' daily life activities by minimizing their reliance on others and enhancing their mobility. Generally, a person who has had a lower leg amputated will be given a prosthesis to help them regain movement. Ideally, a prosthetic foot should perform identically like a healthy human foot (Perry and Burnfield, 1992). A foot prosthesis should deliver shock absorption, compliance on rough ground, push-off, and stride shortening in a lightweight and low-maintenance device. (Lusardi et al., 2013). However, passive foot prostheses still dominate the market and do not incorporate a segmented foot. Clinical researchers demonstrate that ankle-foot amputees who wear passive prostheses face several locomotion difficulties, asymmetric motion, slow-footed walking velocity, and have a greater metabolic cost of walking compared to healthy individuals (Molen, 1973; Winter and Sienko, 1988; Colborne et al., 1992).

Addressing the issues discussed above, powered or active ankle-foot prostheses are developed to generate positive force and control join impedance to propel amputees forward throughout the gait cycle in the attempt to mimic healthy foot (Sun et al., 2018). A few years ago, researchers began to advance the design of powered ankle-foot prostheses. A spin-off company of the University of Malaya, known as BioApps, has started developing a powered ankle-foot prosthesis model, known as BioApps RoMicP®. The BioApps RoMicP® ankle-foot prosthesis is a prosthesis with a motor-based Series Elastic Actuator (SEA) that has been developed to restore leg mobility after amputation.

One of the major components of the SEA system in BioApps RoMicP® prosthesis is the planar rotary spring. The main function of the planar rotary spring, such as mechanical flexible couplings, is to endure minor nonlinearities and loadings from the side. Its primary function is to apply a specified rotational stiffness to achieve the targeted performance of the actuator. Generally, planar rotary spring designs are intended to connect the motor to the output link and are not intended for high torque or low torsional stiffness applications. Thus, this study focused on new design of the rotational compliance of the actuator.

1.2 Problem Statement

SEA is an excellent option for powered ankle-foot prosthesis. However, to achieve the best actuator performance, the optimum stiffness of the planar rotary spring should be defined by using a dynamic mode. The primary purpose of this study is to design a planar rotary spring with the optimum torsional stiffness value. Subsequently, the spring's material and topological shape was selected following the international mechanical design standard.

Finite element analysis is a technique commonly used in the mechanical design verification process. After the design progress has completed, the preliminary spring design's reliability was evaluated.

1.3 Research Objective

To address the challenges associated with the BioApps RoMicP® Foot Prosthesis, this study focused on the design and optimization of the planar rotary spring model through the following objectives:

1. To calculate the required stiffness of planar rotary spring according to the requirement of powered ankle-foot prosthesis.
2. To model an effective design with appropriate material and topological shape.
3. To simulate the stiffness of spring via the method of Finite Element Analysis (FEA) to verify the design.

1.4 Potential Impact of the Research

Amputation results in permanent disfigurement. Relief from pain or diseases in the afflicted limb may be welcomed for some, but resentment is justifiable for individuals who have lost a healthy leg. Amputation brings a physical and psychological impact on for most individuals, and also leads to a substantial financial impact, contributing significantly to the global rise in the cost of healthcare systems, with the annual cost of lower-limb amputation rehabilitation management exceeding USD 4.3 billion in the United States. (Moxey et al., 2011).

A powered ankle-foot prosthesis, known as BioApps RoMicP® is developed to mimic human sound leg closely. This project is directly integrated into the ongoing development project of BioApps RoMicP®. It is expected that the result of this project can positively impact the performance of the ankle-foot prosthesis. This project may also trigger the continuous development to the toe artificial joint mechanism as well as to encourage the development of compliant prostheses and humanoid robots.

1.5 Thesis Organization

Chapter 1 covers the introduction of this project, the overview, the problem statement, the potential impact, and the thesis organization of this final project

Chapter 2 explores the literature on prior research linked to this study It begins with a brief overview if the gait phase and ankle joint mechanism. Subsequently the existing design of powered ankle-foot prosthesis and planar rotary springs is discussed in this chapter.

Chapter 3 covers the methodology of defining the optimum stiffness for the rotating SEA system based on the dynamic model. Subsequently, the procedure of designing the planar rotary springs (by using SolidWorks) and the simulation model (by using Ansys) is explained in this chapter.

Chapter 4 demonstrates the result of the optimum stiffness calculation from Matlab Simulink and illustrates the preliminary design of the planar rotary spring. Moreover, the result of finite element analysis is also attached in this section.

Lastly, Chapter 5 summarizes the finished study and makes suggestions for further academic and commercial endeavors.

CHAPTER 2: LITERATURE REVIEW

2.1 Biomechanics of Human Walking

Biomechanics of human movement has been a subject of study for millennia, but its popularity has exploded in the past fifty years. Numerous research articles have been published on the examination of the human body's biomechanical features during walking. Human walking is a cyclic series of body actions that progress the location of a person. Assuming that all walking cycles are approximately identical, evaluating a single walking cycle simplifies researching the walking process (Alamdari and Krovi, 2017).

Walking is one of the earliest forms of human mobility. Although it seems to be a simple action since it is performed subconsciously, it is one of the most complicated movements performed by human bodies. The purpose of walking is to transmit body weight safely and efficiently across levels or uneven terrain. Throughout walking, the whole neuromuscular system attempts to resist the effects of all external pressures in order to maintain balance. While walking, Bertomeu-Motos (2016) stated in his article that humans will normally do the following steps to guarantee the body is transferred safely and effectively.:

a. Maintaining a balanced and straight bodily posture.
b. Maintaining a safe distance between the feet and the floor by controlling the trajectory of the lower limbs and making a soft touch with the ground.
c. The formation of mechanical energy in order to control the speed in the direction of movement.
d. Absorption of shock forces to maintain bodily equilibrium.

All of these characteristics contribute to the body's actuation and limitations during walking. All bodily components cooperate together to modulate stresses and torques during locomotion, resulting in a smooth and unconscious movement.

2.1.1 Gait Cycle Terminology

Normal human walking can be described using a manner similar to the double pendulum. During forward propulsion, the leg that leaves the ground swings forward from the hip. This is the first swing of the pendulum. The heel of the leg then hits the ground, rolling through to the toes in an inverted pendulum motion. The two legs move in tandem, with one foot in continual contact with the ground (Alamdari and Krovi, 2017).

Gait analysis has been used to provide quantitative data on the kinematics and kinetics of human walking for more than a century. Initially, gait analysis was often based on experimental observations to investigate kinematics and kinetics. Historically, gait analysis was used to gather data in order to get a better understanding of control, improve performance, diagnose movement abnormalities, and evaluate treatment and rehabilitation programs. Thus, clinical gait analysis is defined as the process of gathering and evaluating biomechanical gait data in order to get a better understanding of the effects of sickness and dysfunction (Whittle, 2002).

Baker (2006) stated that clinical gait analysis is performed for four reasons: to differentiate between disease entities (diagnosis), to monitor the progress of a patient's condition, either following or in the absence of intervention, to assess the severity, extent, or type of an illness or injury (assessment), and to predict intervention results (or the absence of intervention). This sort of data may be gathered by gait analysis, allowing for the identification of an effective rehabilitation therapy approach. For efficient gait analysis, it is necessary to employ clear and consistent language. To accomplish this objective, it is critical to first identify and characterize the gait cycle and its phases.

The gait cycle can be defined as the time interval between two consecutive occurrences of the same recurring event during walking. This event can, for instance, be the moment the right foot touches the ground. The gait cycle can be subdivided into two periods for each leg, i.e.: the stance and the swing period. The stance period is defined by the contact between the leg and the ground, and during the swing period, there iss no contact with the ground. The stance is about 60% of the total cycle. This indicates that there is an overlap between the stance periods of the two legs, and during 20% of the gait both legs have ground contact.

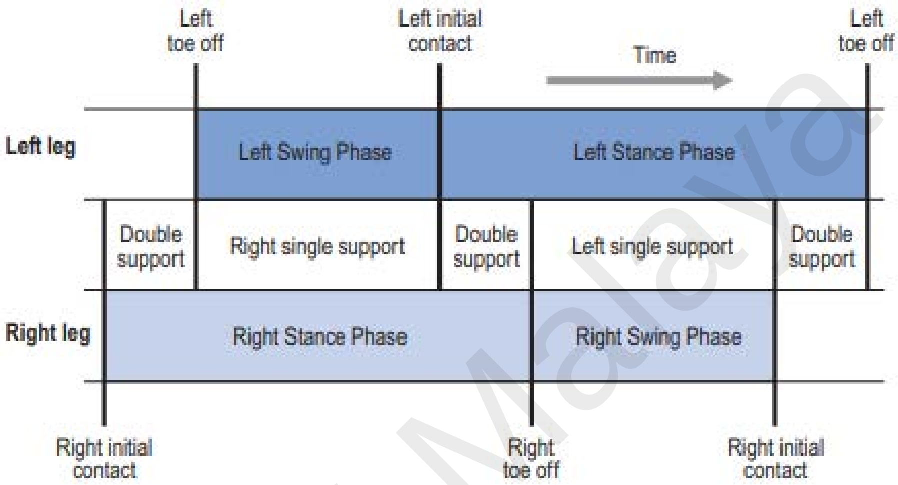

Figure 2.1: Timing of single and double support throughout the period of slightly more than one gait cycle, beginning with the right first contact

The limbs' motion is characterized in terms of reference planes such as the sagittal plane, the frontal plane, and the transverse plane, (Figure 2.1). The sagittal plane is any plane that divides part of the body into right and left portions. The frontal plane divides a body part into front and back portions. A transverse plane divides a body part into upper and lower portions. The majority of this study was projected onto the sagittal plane.

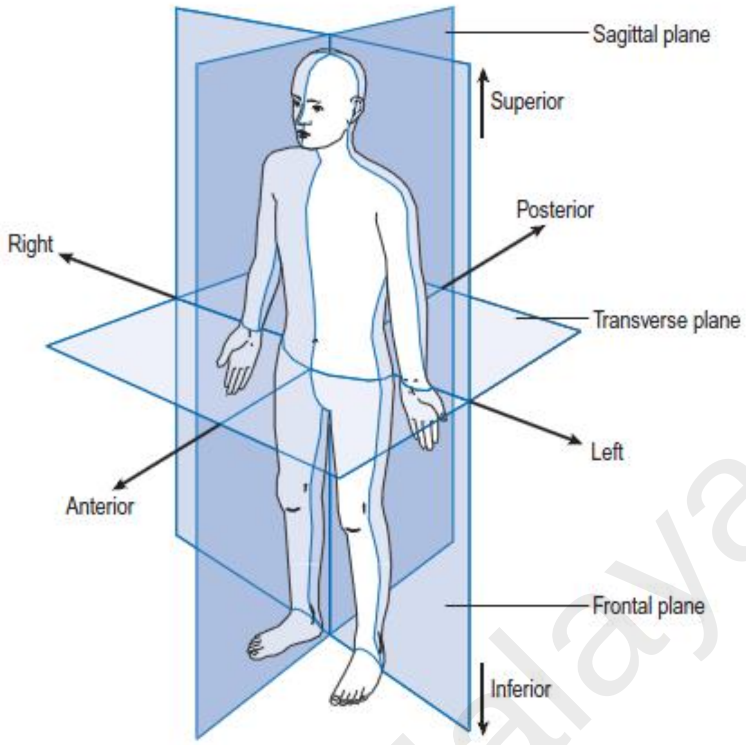

Figure 2.2: The anatomical position and orientation with the three reference planes

The stride and step length are the phrases used to identify the placement of the feet on the ground. The stride length is the distance between two consecutive foot placements. It is composed of two step lengths, left and right, each of which represents the distance traveled by the specified foot in front of the other. It is usual for the two step lengths to be varied in disordered gait. When the left foot is pushed forward to take a step and the right foot is brought up alongside it rather than in front of it, the right step length is zero. It is even feasible for one foot to have a negative step length if it never catches up to the other. However, unless the subject is walking around a curve, the stride length recorded between subsequent left foot positions must always be the same as the stride length measured between successive right foot positions.

As with distance, there are a few key terminologies for describing time and speed in connection to the human gait. The number of steps taken by an individual during a certain period of time is referred to as his cadence. The issue with this variable is that it measures half cycles per unit of time, which is not deemed scientifically acceptable. Another explanation is that, the left and right steps are not always comparable in size for individuals with disordered gait. It is preferable to calculate the cycle time or stride time, which is the time required for an individual to take two steps or one stride. Its relationship to the cadence is as follows (Eq. 2.1):

$$Cycle\ time(s) = \frac{120}{Cadence\ \left({}^{steps}/_{minutes}\right)} \tag{2.1}$$

If the length of one step is divided by this cycle time, the walking speed can be calculated by the following formula (Eq. 2.2):

$$Speed\ \left({}^{m}/_{s}\right) = \frac{Stride\ length\ (m)}{Cycle\ time(s)} \tag{2.2}$$

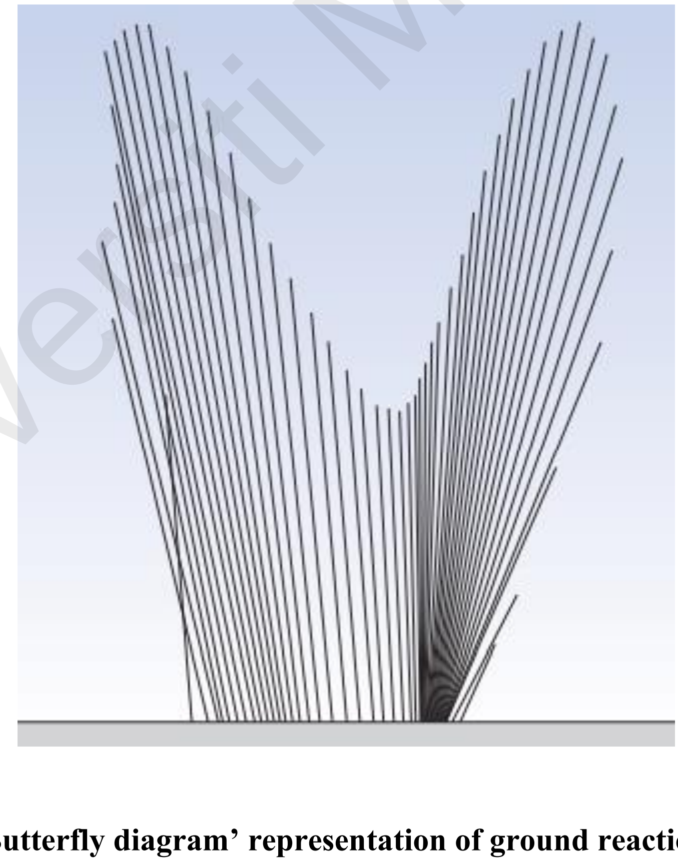

Figure 2.3: 'Butterfly diagram' representation of ground reaction force vector at 10 ms intervals. Progression is from left to right.

The forces involved in the gait cycle can be characterized in various methods. Pedotti (1977) proposed the butterfly diagram, a method for plotting horizontal and vertical pressures against time, either in seconds or as a percentage of gait. Figure 2.3 illustrates successive representations of the ground response force vector's magnitude, direction, and point of application at 0,01 seconds intervals. The vectors traverse the graphic in a left-to-right direction.

2.1.2 Key Phases in Gait Cycle

The gait cycle is often described in further depth by identifying eight distinct stages, five during stance and three during the swing. Heel strike, loading response, mid-stance, terminal stance, and pre-swing happen during stance, whereas acceleration, mid-swing, and deceleration occur during the swing.

1. Initial contact (0% to 2% of the gait cycle). The initial contact is the beginning of the loading reaction or weight acceptance. It also marks the start of the stance phase and the first segment of the initial double-leg support period. During this period, any impact phenomena will also be present (Figure 2.4).

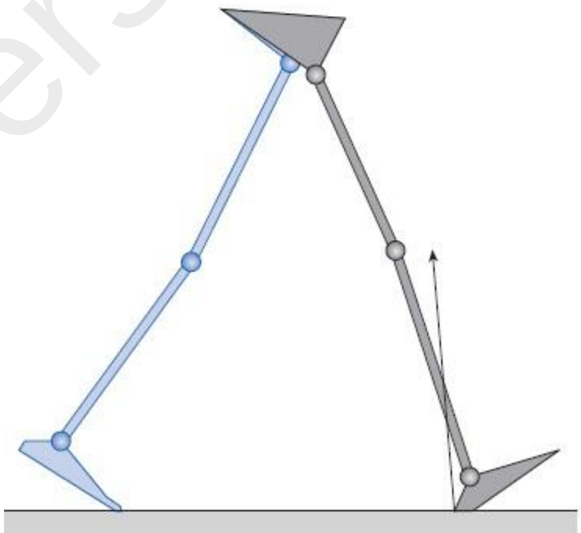

Figure 2.4: Initial contact. The arrow represents the ground reaction force

2. Loading response (2% to 12% of the gait cycle). The remaining of the first double-leg support time is the loading reaction. During this phase, we continue and finish the

weight acceptance job. The human gait has the least (or greatest) braking peak in terms of anterior-posterior force. The human gait has the presence of the lowest (or maximum) braking peak in terms of anterior-posterior force (Figure 2.5).

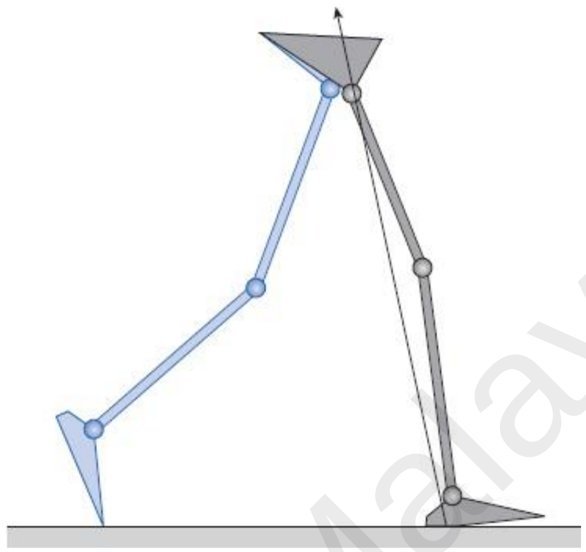

Figure 2.5: Loading response

3. Mid-stance (12% to 31% of the gait cycle). This marks the beginning of the time of single-leg support. Stability is a key problem since the base of support will be substantially reduced and the center of gravity will be at its greatest position due to leg extension. Kinetic energy is converted to potential energy. The appearance of the 'valley', or the local minimum of the vertical ground reaction force, marks the conclusion of this phase (Figure 2.6).

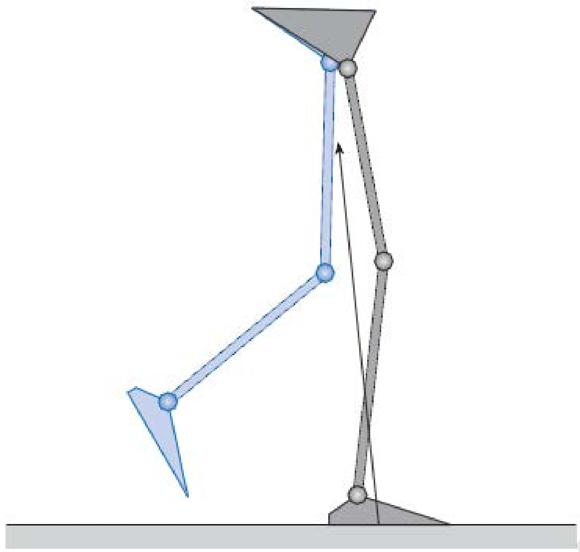

Figure 2.6: Mid-stance

4. Terminal stance (31% to 50% of the gait cycle). The second phase of the single-leg assistance period has begun. Stability is still an issue, as is the opposing foot's heel strike. The center of gravity ‘falls’ from its highest point, converting potential energy to kinetic energy (Figure 2.4).

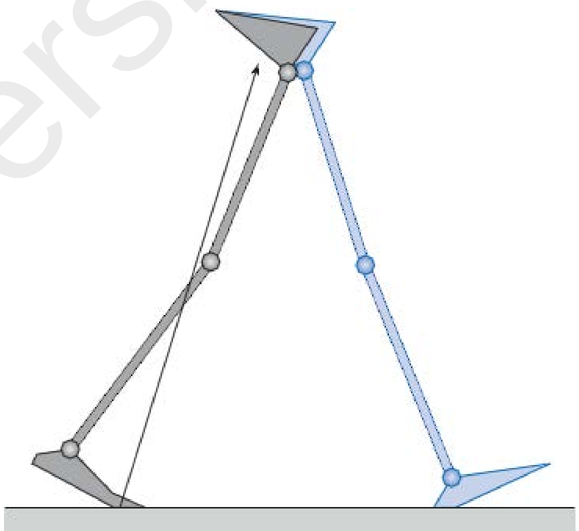

Figure 2.7: The initial contact of the other foot. This is the event that separates terminal stance from pre-swing

5. Pre-swing (50% to 60% of the gait cycle). This is our second loading phase and the terminal double-leg support period. We have the occurrence of the second loading

peak, the second local maximum, or the second "hump" in terms of vertical ground reaction force. We also have our highest propulsion peak in terms of anterior posterior force during this phase as we prepare to launch our foot off the ground (Figure 2.8).

Figure 2.8: Toe off. This indicates the end of the pre-swing phase

6. Initial swing (60% to 73% of the gait cycle). This is the initial phase of the swing period, and our primary goal is to clear the floor by flexing the entire leg. This total flexion reduces the moment of inertia of the leg while increasing the angular velocity of the swinging leg.
7. Mid-swing (74% to 87% of the gait cycle). This is the second portion of the swing phase, and our main concern is that our opposite/contralateral leg is in single support with a limited base of support, causing instability. We are also preparing for the foot impact at the end of our swing (Figure 2.9).

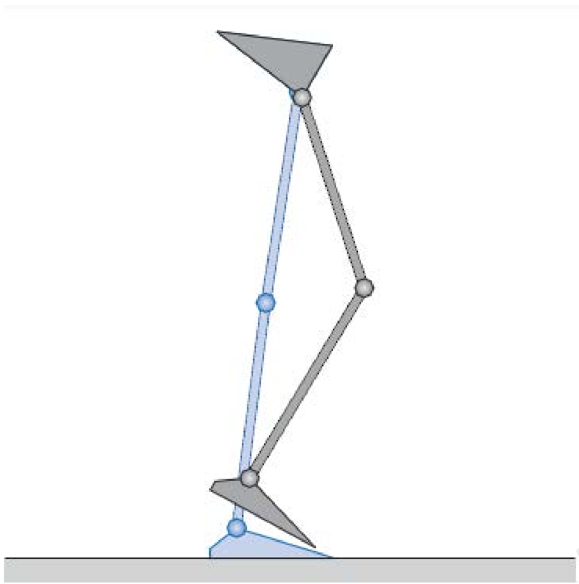

Figure 2.9: The center of the swing phase. The two feet are next to each other

8. Terminal swing (85% to 100% of the gait cycle). This is the third and last section of the swing, and our main issue is the approaching foot contact.

2.2 Biomechanical Behaviors of ankle

2.2.1 Anatomical References Planes and Axes

As discussed before, three anatomical reference planes may also be used to describe the foot (Figure 2.10,at the left side). When the body is in its anatomical reference position, all anatomical reference planes cross at a single location, referred to as the body's center of mass or center of gravity (Hall, 2012). The midline axis of the foot extends from anterior to posterior (Mann, 1985).

The whole body may move parallel to or along an anatomical reference plane, but individual body segments can move in the sagittal plane, transverse plane, or frontal plane, which can occur at or in a plane parallel to the sagittal, transverse, or frontal planes, respectively (Figure 2.2). When a body segment moves, it rotates along an imaginary rotation axis that goes through the joint to which it is linked. Indeed, in addition to the three anatomical reference planes, there are three anatomical reference axes, each parallel to one of the three planes. The mediolateral axis is perpendicular to the sagittal plane, the longitudinal axis to the transverse plane, and the anterior-posterior axis to the frontal plane. Thus, rotation occurs along the mediolateral, longitudinal, and anteroposterior axes in the sagittal, transverse, and frontal planes. Thus, dorsiflexion and plantarflexion occur along the mediolateral axis, abduction and adduction occur along the longitudinal axis, while eversion and inversion occur along the anteroposterior axis. All of these characteristics are presented in Figure 2.10.

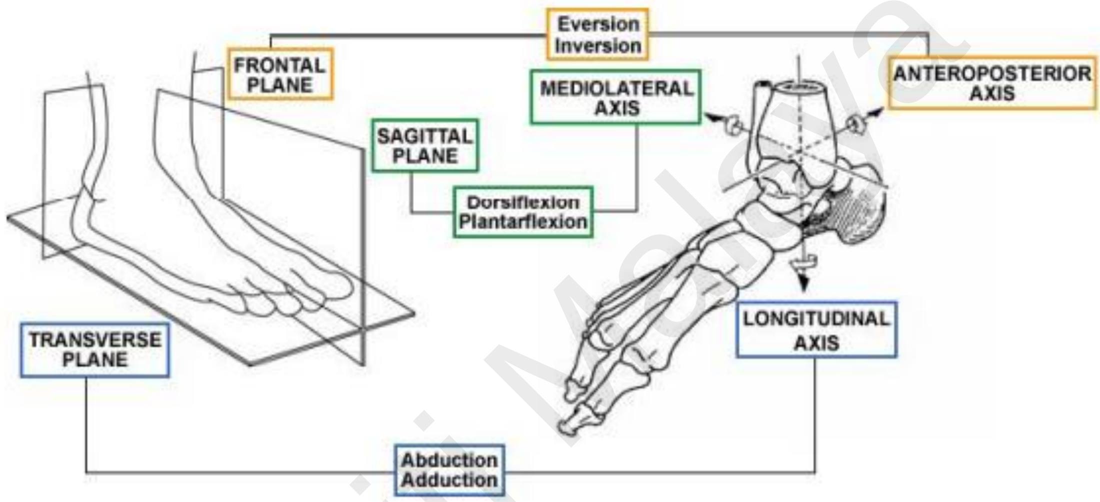

Figure 2.10: The anatomical reference position of the foot and the three anatomical reference planes (left). The three anatomical reference axes applied to the ankle joint (right) (adapted fromRodrigues, 2013)

2.2.2 Joint Motion Terminology

The majority of human movements are classified as "general motions," which include linear (translational) and angular (rotational) motions. When the human body is in its anatomical reference position, all body segments are regarded to be at 90 degrees to one another. Given this, the rotation of a body segment away from its anatomical reference position is denoted by the direction of motion and quantified by the angle formed between the body segment's location and the anatomical reference plane (Hall, 2012).

The foot, particularly the ankle joint, moves in three anatomical planes. The sagittal plane contains dorsiflexion and plantarflexion actions, the transverse plane contains abduction and adduction motions, and the frontal plane contains eversion and inversion motions – shown in Figure 2.10 (Sammarco and Hockenbury, 2001). There are two-more-foot movements: pronation and supination, both of which include simultaneous motion in three planes (sagittal, frontal, and transverse) and are hence referred to as "tri-plane motions." Figure 2.3 summarizes all conceivable foot actions. Each action is described in detail in Figure 2.11.

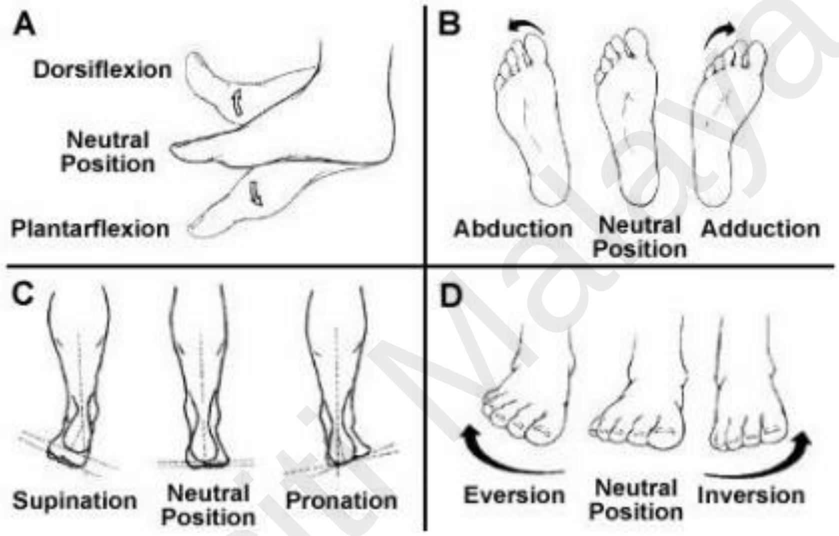

Figure 2.11: Ankle joint motions

Dorsiflexion describes the movement of the foot when the toes are raised off the ground, while plantarflexion refers to the movement of the foot when the toes are pressed against the ground. Adduction, on the other hand, refers to the action of bringing anything closer to the body's midline (medial rotation), and abduction refers to the motion of moving something away from the body's midline (lateral rotation). Inversion and eversion are terms that refer to the internal rotation of the foot when it rolls over to the medial side of the body, whilst the latter occurs as the foot rolls over to the lateral side (external rotation). Finally, pronation is a combination of abduction, eversion, and dorsiflexion and involves the movement of the foot upward and away from the body's center (the plantar surface faces laterally), whereas supination is a combination of adduction, inversion, and plantarflexion and involves the movement of the foot downward and toward the body's center (the plantar surface faces laterally) (the plantar surface faces medially) (Michael et. al, 2008; Hall, 2012; Schumacher, 2012)

2.3 Powered Ankle-foot Prostheses: State of the Art

According to Black's Medical Dictionary (van Oort, 2011), a prosthesis is "an artificial substitute for a missing or dysfunctional bodily component." Prostheses are devices that replace body parts after amputation, which is defined as the "severance of a limb, or part of a limb, from the remainder of the body." The word transtibial refers to the lower leg in this circumstance, and the amputation occurred between the knee and the ankle. The tibia is the biggest bone in the lower leg, connecting at one end to the thigh bone and at the other end to the ankle joint.

For thousands of years, foot prosthesis has been used globally. From an engineering standpoint, the three primary kinds of prostheses are outlined, namely passive, semi-active, and active prostheses. Passive prostheses work as a fixed spring and damper and offer only little functionality. Due to microprocessor technology, semi-active prostheses may rapidly adjust their behavior and adapt to changing situations. While they are more adaptable, they are limited in their capacity to generate opposing forces. Active or powered prostheses are those that get external power via motors and hence have the ability to act. While they provide increased performance and functionality, they are also the most complex system (Windrich et al., 2016).

The powered ankle–foot prosthesis has sparked considerable curiosity. Due to the construction of powered ankle–foot prosthesis with driver units, they may provide direct energy for walking. As a result, amputees can walk more easily with powered ankle–foot prostheses than with passive ankle–foot prostheses. Electric motors, pneumatic actuators, or hydraulic actuators are the three primary systems used to power powered ankle–foot prosthetics. Microprocessor-controlled spring-damper devices may enhance the performance of the prosthetic model. However, kinematic and kinetic gait investigations indicate that amputees have a more asymmetric walk and consume more oxygen than healthy people. Persistent gait abnormalities may have long-term consequences (Gailey et al., 2008; Robbins et al., 2009), including decreased living comfort and increased expenditures for the amputee or medical insurance provider. Further advancements in prosthetic design are necessary to avert this.

In the late 1980's, the Belgrade Above Knee Prosthesis (AKP) took the first steps toward powered prostheses (Popovic et al., 1991). External power and control were employed to power and control the system. The knee joint was driven by a direct current motor. The active knee amputee's energy consumption may be lowered while increasing their maximal walking pace.

The Proprio Foot was the first commercially available active foot (Figure 2.12(g)). It has the capability of lifting the toe during the swing phase in order to adjust to the terrain and avoid accidents or falls. Accelerometer and angle sensor are attached to the system in order to detect environmental conditions around the user (stairs, slope, flat, sitting, or standing). Moreover, a linear actuator is placed to match the specified ankle angle to correspond to the specified angle. Thus, take-off and landing motions can be well-recognized. Additionally, the last stage is considered to improve pattern recognition. A similar actuation approach was utilized to present the notion of the prosthetic ankle by Svensson and Holmberg (2006).

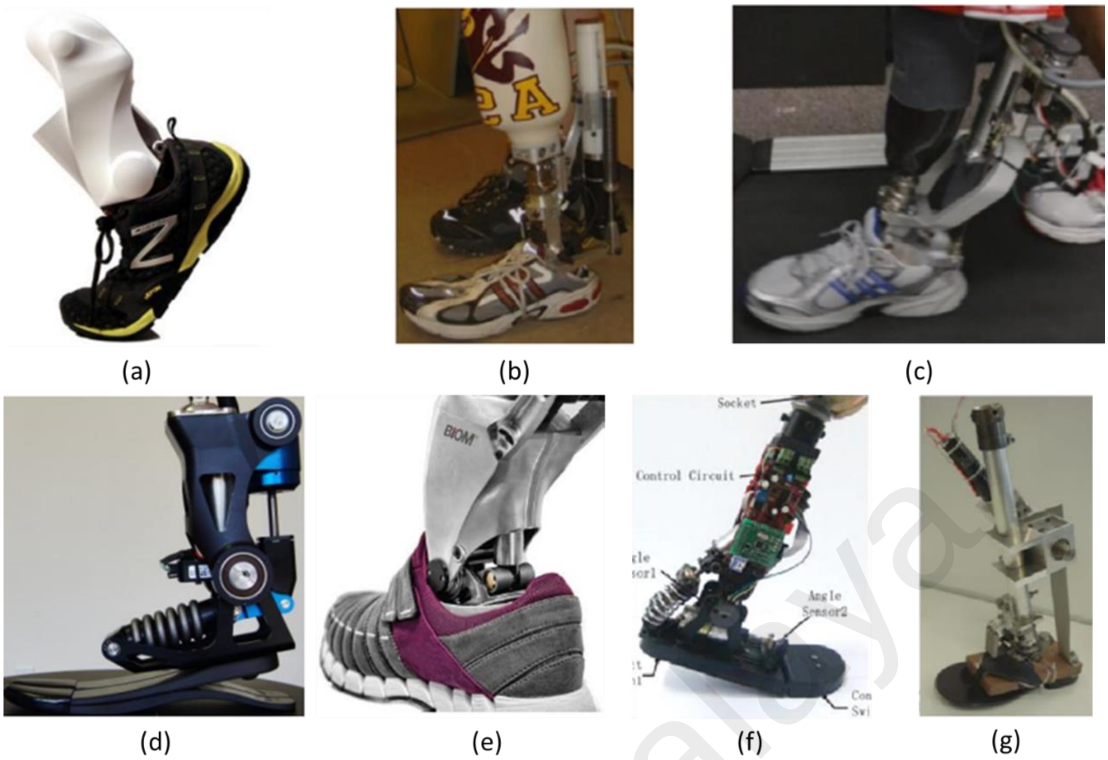

Figure 2.12: Active ankle foot prostheses

iWalk is another example of marketed design for an active foot (Figure 2.12(e)). They presented the BiOM Power Foot to serve as a substitute for the ankle joint. The elastic function (spring) of the Achilles tendon is paired with a motor that mimics calf muscle action. This approach enables not just swing phase adaptations, such as with the Proprio Foot, but also active powered push-off.

Springactive and Westpoint Military Academy (Hitt et al., 2010a) modeled powered ankle joints for walking (Figure 2.12(a)) and running (Figure 2.12(c) and (d)) based on prior designs (Figure 2.12(b)) from Arizona State University (Bellman et al., 2008). An actuated toe joint is also included in the foot prothesis – called PANTOE 1 (Figure 2.12(g)) – which was developed by the Peking University (Zhu et al., 2010; Yuan et al., 2011).

Liu et al. (2021) has classified and compared the mechanical design of prototypes and commercialized lower-limb prostheses into several subdivisions. Briefly, they categorized powered ankle-foot prosthesis into three types based on its actuation system, namely hydraulic actuators, pneumatic actuators, or electric motors. Due to their high energy density, the first two kinds of actuators can supply adequate ankle torque and power. Pneumatic actuators, on the other hand, need a gaseous input/output medium, whilst hydraulic actuators must overcome seal and circuit arrangement constraints. Due to the limits of pneumatic and hydraulic actuators, prostheses powered by these kinds of actuators cannot be readily decreased in size. As a result, applicability for everyday usage is limited.

2.3.1 Actuator Concepts

All commercially available active foot prostheses and most prototypes drive the ankle or knee joint with electrical motor technology. Furthermore, several of them use various types of elastic principles. Motor and elastic element alignments in series, parallel, or unidirectional parallel are utilized to reduce motor needs. Peak power (which is linked to motor size) and energy needs (which is linked to battery size and operating duration) are two features that should be reduced in contrast to direct drive (DD) systems. Most active foot prosthesis prototypes attempt to replicate the ankle and knee joint torque ankle characteristics. Several of them operate with low power (Svensson and Holmberg, 2006; Fradet et al., 2010) to adjust ankle angle for ground clearance during off-ground phase or adapt ankle angle to slopes.

Additionally, hydraulic or pneumatic actuators might provide a better power density than electrical motors. Pillai et al. (2011) showed a concept that utilizes linear hydraulic actuators powered by a single pump to provide energy injection for the ankle and knee joints. As a result, push-off may be supported at the ankle, the knee, and the ankle joint. The knee may be propelled during stair ascending and late swing. A unique aspect is its ability to function in active mode or as a semi-active device, similar to the C-Leg.

The pleated pneumatic artificial muscles (PPAM) design can be used to showcase pneumatic actuation (Versluys et al., 2009). The technology could produce the torques necessary for walking with a prosthetic ankle joint. In the laboratory, PPAM pressure was created using a stationary compressor. Using PPAM, it is feasible to change the stiffness for various speeds. A linear regression on human ankle torque-angle curves was used to determine the required stiffness. A similar pneumatic system is applied for tests with orthotic structures (Ferris et al., 2005; Sawicki and Ferris, 2009).

2.3.2 Spring Configuration

It is possible to identify suitable elastic actuator setups for various leg joints and various tasks. The aim is to find the most versatile solution that may be used in various everyday life tasks. The primary emphasis should be on daily activities such as walking or even standing still in terms of energy usage. However, energy and power need to be associated with stair climbing, standing, sitting, walking slopes, or sprinting might also be considered when selecting an elastic actuation model.

Different actuator options might be proposed as a result of muscle simulation. In this study, solutions using SEA were employed (Pierrynowski and Morrison, 1985). Parallel elements (PE) to the contractile element (CE) were removed from this analysis because of several reports of minimal parallel forces. In comparison, the Hill Model incorporates both a SE and a PE. There are many other possible options, such as combining the CE and SE in conjunction with the PE (Zajac et al., 1989) in Figure 2.13(e), or using simply the CE in parallel with the PE (Nigg et al., 1994) (Figure 2.13(c)). Along with standard elastic models, unidirectional springs that activate under specified conditions (kinematic, kinetic) could be explored.

Sup et al. (2009) introduced a method where the spring is activated at an ankle angle of about five degrees plantarflexion. The BiOM ankle prosthesis (Eilenberg et al., 2010) incorporates a SEA, extending the system to a configuration similar to that shown in Figure 2.13(i). The unidirectional spring is specified as being engaged at zero degrees in an older version of the device (Au et al., 2009). Sparky's Robotic Tendon method incorporates a series spring (Figure 2.13(b)) with a far lower stiffness than the BiOM ankle. Calculations of power optimization can perform to determine stiffness (Hollander and Sugar, 2005). This design variance is due to the length of the lever arm connecting the ankle joint to the actuator (Grimmer and Seyfarth, 2011b).

In comparison, the BiOM ankle series uses an open-loop force bandwidth to determine the stiffness (Au et al., 2009). Hitt et al. (2010a) and Schinder et al. (2011) employed a method where two parallel elastic actuators were added to the design to provide the needed power requirements during operation.

The AMP foot 2.0 is similarly constructed using a series spring technique (Cherelle et al., 2012). Compared to techniques that need more than 150 W motors, this solution uses just a 60 W motor. This solution is attainable via the combination of two fundamental processes. The little motor loads a series spring with consistent force during the stance phase, decoupling it from ankle motion. A second spring conserves energy in the same manner as the forefoot portion of the Energy Storing and Return Prosthetic (ESAR) feet does. The passive spring recovers its energy during push-off.

Additionally, a clutch is employed to dissipate the energy generated by the motor-spring combination (Figure 2.13(f)). On the one hand, this strategy has the benefit of requiring less peak power from the motor. The approach might reduce space and weight, provided the clutch mechanism is sufficiently compact. In contrast to Eilenberg et al. (2010) and Hitt et al. (2010b), the energy return cannot be controlled in the same manner. It is similar to a catapult in that it only releases energy when the trigger is pushed. The interface with the amputee must be adequately designed to follow specific patterns. More research should be carried out to the extent to which this strategy is adaptable to other daily life conditions such as varying speeds, slopes, and stairs.

The PANTOE 1 employs two SEAs (Zhu et al., 2010; Yuan et al., 2011). The ankle prosthesis incorporates a single SEA for plantar and dorsiflexion of the ankle. Another SEA is involved in the toe joint motion control. The active prosthetic toe joint is expected to enhance various biomechanical characteristics of the foot, including a range of motion, angle velocity, and energy output. In comparison to rigid foot design, faster walking velocities should be attained.

For the ankle (Grimmer and Seyfarth, 2011b; Wang et al., 2011; Eslamy et al., 2012; Grimmer et al., 2012), the knee (Grimmer and Seyfarth, 2011a; Wang et al., 2011), and the hip (Wang et al., 2011), systematic analyses on elastic actuator concepts that reduce energy requirements (ER) or peak power (PP) have been published. Calculation methods are based on Hollander and Sugar (2005). To save energy, the actuator velocity or force might be lowered. A series spring can reduce the motor's speed. A parallel spring is capable of reducing the force applied to the motor.

Significant motor improvements may be recognized for the ankle joint when a series spring with optimum stiffness is used instead of a direct drive. The average benefit in terms of energy requirement (ER) was around 64.7% for running and 25.8% for walking utilizing a SEA at five different speeds ranging from 0.5 to 2.6 m/s. A Parallel Elastic Actuator (PEA) (Figure 2.13(c)) may have a lesser effect on ER. 45% and 12.2%, respectively, were conceivable. The Combination of two elastic structures (SE+PEA, (Figure 2.13(d)) results in a 52.8% energy advantage for running and a 17.9% energy advantage for walking for the elastic actuator.

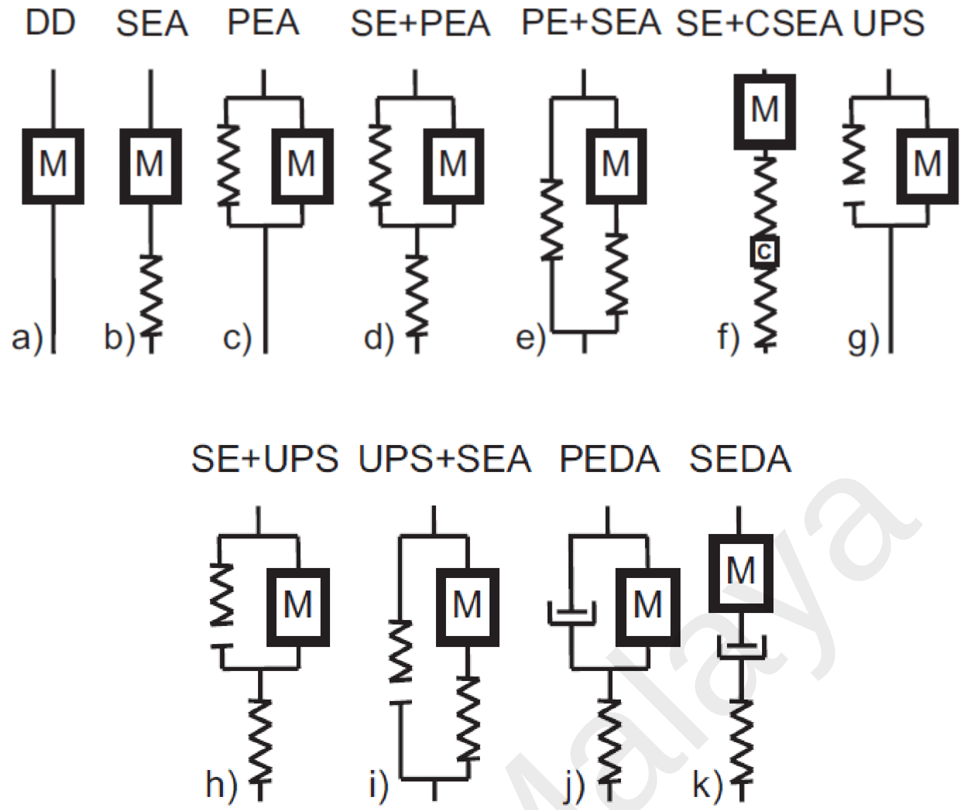

Figure 2.13: Various concepts for elastic actuators

The SE+PEA (Series Elastic and Parallel Elastic Actuator) system achieved the most significant savings (81.8%) when operating in peak power consumption. The parallel spring's force reduction is the most significant factor in lowering power consumption. A single PEA already had a mean advantage of 79% over the five speeds. In operation, a SEA might cut PP by 68.5%. A similar pattern was seen with walking. SE+PEA provided the most advantages (70.4%). The PEA (62.5%) and the SEA had lower advantages (48.3%).

Parallel unidirectional springs at the ankle joint (Figure 2.13(g), (h), and (i)) may provide comparable power gains to the PEA. Additionally, some speeds may have a smaller ER than PEA (Eslamy et al., 2012).

A SEA may provide energy advantages of 5% to 29% while walking (0.5 m/s to 2.6 m/s) at the knee joint. When negative work must be performed by the motor, little or no

PP (high speeds up to 31%) reductions were feasible in walking (no passive damper or energy harvester to perform negative work). For running (0.5 m/s to 4 m/s), energy savings of 40% to 71% and PP savings of 54% to 78% were discovered.

Calculations of probable decreases in the hip joint were performed for walking at 0.8 m/s and 1.2 m/s. A PEA has been shown to lower torque by 66% in flexion and extension. At the hip, a 53% loss in abduction and adduction was detected (Wang et al., 2011). Utilizing a SEA, it was possible to identify torque reductions of 60% for the same motion.

2.3.3 Damping

Along with springs, dampers may assist in minimizing the number of actuators required in a powered lower limb prosthesis. These passive prosthetic components have the potential to introduce negative joint power. Due to microprocessor-controlled mechanisms, semi-active prosthetic knee joints can adjust the damping ratio in response to changes in walking speed. It is possible to replace abnormal muscle function. A motor capable of decelerating the motion may perform a similar job.

When a damper is used to lower the energy needs for a motor in a prosthetic ankle joint comparable to the eccentric phases of the knee joint, it is feasible to reduce the energy requirements for the motor. Possible surgery stages include those associated with the replacement of tibialis anterior function upon touch down. Additionally, when descending stairs, the negative effort may be accomplished by using a damper to simulate eccentric plantar flexor action. Eslamy et al. (2013) estimated gains of up to 50% for power peak and around 26% for energy needs compared to a pure SEA (Figure 2.12(k)). Similar ideas for a motorized ankle joint integrating motors, springs, and dampers may be found in a 2012 patent (Herr et al., 2012). No advantage of a continuous functioning damper could be demonstrated for level walking in any studied system (Eslamy et al., 2013). Controllable dampers that are activated at certain gait phases might affect the findings.

If the assistive damper is only necessary during some portions of the gait cycle, it should be switchable to minimize adverse effects during other phases. A damper that simulates the function of a heel pad or wobbling mass may be active throughout the gait cycle.

2.4 Series Elastic Actuator

Numerous actuation methods were explored in the preceding chapter, with most of them applying to powered foot-ankle prosthetic models. The type of actuation employed in this study is a series elastic actuator. A Series Elastic Actuator (SEA) is an energy storage device consisting of an elastic element coupled in series to an actuator. This elastic element offers impact load tolerance, decreased mechanical output impedance, passive mechanical energy storage, and increased peak power output for SEAs. The MIT Leg Lab has spent the past decade focusing on a revolutionary series elastic actuation. Pratt and Williamson presented a SEA with a structural torsion spring and a locally positioned geared motor to offer accurate and consistent force control, less reflected inertia and higher shock tolerance (Hurst and Green, 2020) (Figure 2.14).

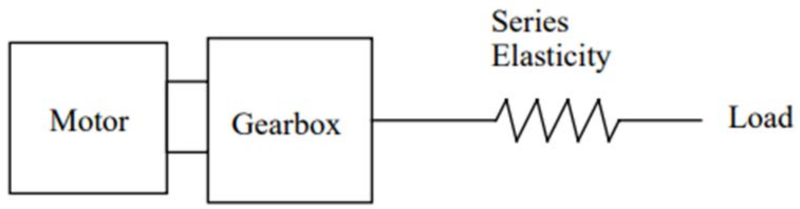

Figure 2.14: The Schematic Series Elastic Actuator as introduced by Pratt and Williamson (1995)

The MIT actuators have a low-damping, series-spring configuration with a modest level of stiffness. These systems, in particular, lack the suppleness necessary to reproduce animal-like series stiffness and the associated energy storage patterns associated with running gait. However, the devices are very flimsy compared to a load cell (a popular "compliant" element used in force control applications). Due to the moderate compliance between a highly geared actuator and the load, the MIT-style series elastic actuator (MIT-SEA) is mainly suited for force control applications. It is capable of dealing with rapidly changing force loads. Compared to a conventional gear motor, the risk of transmission damage in the event of a collision is significantly reduced (Pratt and Williamson, 1995).

Numerous characteristics of an actuator lost when gears are installed can be recovered via series elasticity. Series elasticity acts as a low-pass filter for shock loads, significantly reducing peak gear forces. While the same low-pass filter that spreads out a shock impulse back driving the actuator also spreads out the actuator's output, this is a trade-off in engineering, not a one-sided reduction. A sufficiently flexible interface can considerably enhance shock tolerance while still providing for an acceptable amount of micromotion bandwidth.

Series elasticity turns the force control problem into a position control problem, considerably improving force accuracy. A series elastic actuator's output force is proportional to the difference in position across the series elasticity multiplied by the spring constant. Since the position is simpler to control accurately via a gear train than force, reducing the interface stiffness decreases the force errors caused by gearing.

Increased series elasticity facilitates the achievement of stable force management. In contrast to position control, difficulties improve when the frequency of the interface resonances is lowered. The motor's force-feedback loop may operate well at low frequencies, resulting in an effective zero-rate spring in series with the interface. Because zero-rate springs prevent the motor and load inertias from resonating, the system as a whole becomes stable.

The stability requirement is equivalent to minimum load inertia determined by the robot structure's inherent mass. Since negative masses do not exist in nature, stability is guaranteed when in contact with any object.

Lastly, series elasticity enables energy storage. This energy storage may significantly increase the efficiency of legs movement. Although the elasticity is hidden from the higher-level control system, it may be included in the actuator package to benefit efficiency. In other words, unlike techniques that seek to account for link elasticity at the system level, the high-level control system thinks it is running independent force actuators while the actuators have internal springs that provide the advantages mentioned above.

Various trade-offs dictate the SEA's design, the most often employed are power output, volumetric size, weight, efficiency, back-drivability, impact resistance, passive energy storage, backlash, and torque ripple. For example, electromechanical linear SEAs with ball screw reduction mechanisms are often used because of their high efficiency, impact tolerance, and back-drivability (Pratt et al., 2002; Knabe et al., 2014; Paine and Sentis, 2014). The Shipboard Autonomous Firefighting Robot (SAFFiR) (Orkehov et al., 2013), Tactical Hazardous Operations Robot (THOR) (Lee et al., 2014), M2V2 (Pratt et al., 2008), and Valkyrie (Paine et al., 2015) are some examples of humanoid robots having electromechanical linear SEAs. Rotary SEAs are also the subject of much investigation due to their diminutive size. Rotary series elastic actuators, including harmonic drive reduction techniques, have been included in COMpliant huMANoid (COMAN) (Tsagarakis et al., 2013), Walkman (Negrello et al., 2015), Valkyrie (Paine et al., 2015), and Toro (Englsberger et al., 2014; Paine et al., 2015; Tsagarakis et al., 2015). Cable-driven series elastic actuators allow remote control of a revolute joint, as shown in Roboray (Kim et al., 2013) and Flame/TUlip (Hobbelen et al., 2008; Kim et al., 2013). However, there has been no application of rotary series elastic actuator in foot prosthetics.

Therefore, this study used a rotational actuator system on the powered ankle-foot prosthesis model.

Among the numerous benefits of compliant actuators, including energy storage, shock absorption, and improved force control fidelity, a greater emphasis should be placed on force control fidelity, as accurate force control is required for the prosthesis to interact with the environment stably. While choosing the optimal stiffness value to achieve excellent force fidelity is crucial, only few studies have been undertaken in this area. Robinson, 2000; Paine and Sentis, 2014; Orekhov et al., 2015). There are some published articles on actuator design, but all of them concentrated on linear SEAs.

2.5 Existing Planar Rotary Spring Design

The design of the elastic element is critical as it determines the actuator's maximum large torque bandwidth and forces fidelity. (Stienen, 2009). A considerable amount of research in SEA development has been focused on designing custom components suitable to match the specific requirements of a given application. The spiral-based spring designs shown in Figure 3.4 were established in prior research projects. Figure 3.4(a) was developed by Knox and Schmiedeler (2009), Figure 3.4(b) was developed by Stienen et al. (2010), Figure 3.4(c) was developed by Lagoda et al. (2010), Figure 3.4(d) was developed by Georgiev and Burdick (2017), Figure 3.4(e) was developed by Carpino et al. (2012), Figure 3.4(f) was developed by Paine et al. (2015), Figure 3.4(g) was developed by Cummings et al. (2016) .The spring in Figure 3.4(a) is a single spiral wrapped from a steel strip, while the remainder of the spiral springs are created via electrical discharge machining on a steel plate. Archimedean spirals are used to model the springs in Figures 3.4(b), (c) and (d). The springs in Figures 3.4(a), (b), and (c) were developed using simple spiral torsion spring theory. Meanwhile, the spring in Figure 3.4(d) was developed by using the curved beam theory. The spring in Figure 3.4(e) was created by iterative shape optimization using Finite Element Analysis (FEA). The springs seen in Figures 3.4(f) and (g) operate in the same manner. Previous studies have selected a spring geometry and then modeled it in the FEA system. The FEA study was iterated ad hoc, with tiny modifications to design parameters, until a solution that matches performance standards while remaining within the limits of the packaging has been identified. However, no systematic design approach for such springs that match performance criteria while adhering to geometric design limitations has been published in the literature (Georgiev and Burdick, 2017).

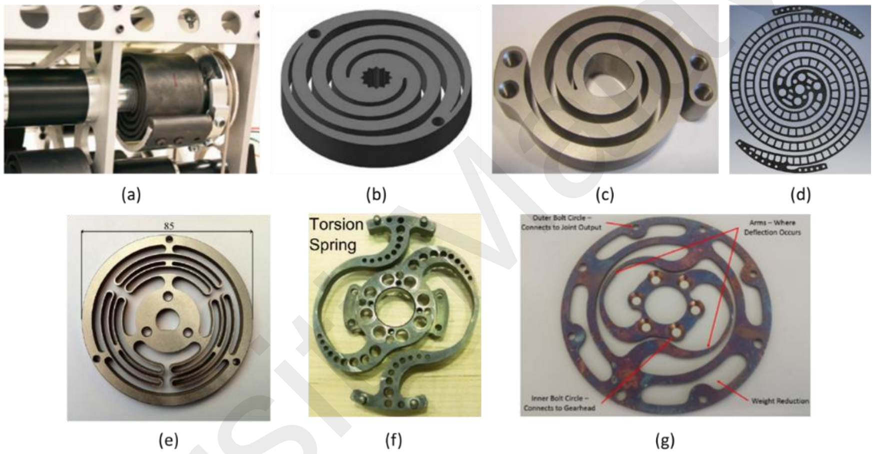

Figure 2.15: Existing planar rotary spring design

Similar to Figures 3.4(a), (b), (c) and (d), this study presents classical, and highly simplified, design of the Archimedean planar rotary spring model. According to Lagoda et al. (2010), the Archimedean planar rotary spring model has the advantage of cancelling out undesired radial forces acting on the spring center when the spring is wrapping or unwrapping.

CHAPTER 3: METHODOLOGY

3.1 Series Elastic Actuator

The purpose of this is to provide schematic diagram of the rotary series elastic actuators for BioApps RoMicP® ankle-foot prosthesis (Figure 3.1).

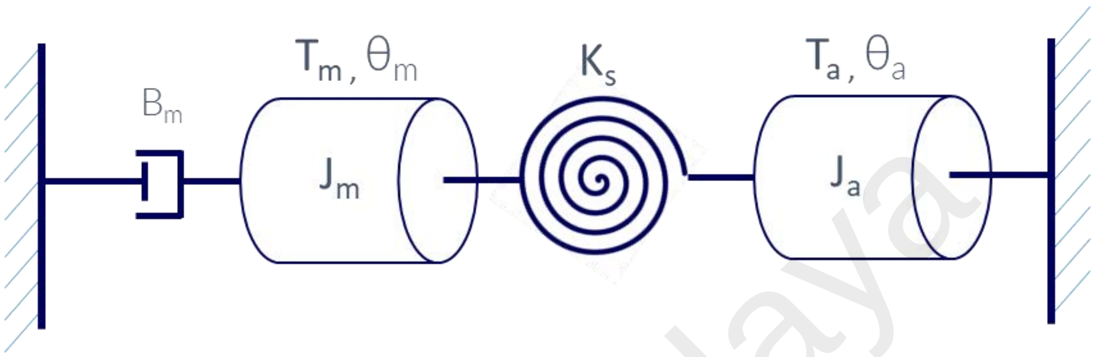

Figure 3.1: The schematic diagram of the rotary series elastic actuators for BioApps RoMicP® ankle-foot prosthesis

The rotary series elastic actuator for BioApps RoMicP® ankle-foot prosthesis includes a damping, motor, planar rotary spring, and output (ankle). There are several parameters applied to the system, i.e., the damping coefficient (B_m), the rotational moment of inertia of the motor and gearhead (J_m), the motor torque (T_m), the motor position (θ_m), torsional spring stiffness (K_s), the rotational moment of inertia of the ankle (J_a), the ankle torque (T_a), and the ankle position (θ_a).

3.1.1 The Dynamic Model of the Rotary Series Elastic Actuator

The torsional spring stiffness affects the dynamics of the system, the torque sensing range, resolution, and the speed at which the system can operate safely. Thus, the choice of an optimum torsional spring stiffness is a critical decision (Cummings et al., 2016). The general dynamics of the rotary series elastic actuator can be derived from the schematic diagram in Figure 3.1 as follows (Eq. 3.1 and 3.2):

$$\ddot{\theta}_m = \tau_m + \tau_b + \tau_s \tag{3.1}$$

$$J_a\ddot{\theta}_a = \tau_a - \tau_s \tag{3.2}$$

$\ddot{\theta}_m$ is the acceleration of the motor, $\ddot{\theta}_a$is the acceleration of the ankle, τ_b is the damping torque, and τ_s is the planar rotary spring torque. Furthermore, the damping torque and the spring torque value can be defined by the following equations (Eq. 3.3 and 3.4):

$$\tau_b = \; - B_m\dot{\theta}_m \tag{3.3}$$

$$\tau_s = \; - K_s(\theta_m - \theta_a) \tag{3.4}$$

$\dot{\theta}_m$ is the velocity of the motor.

3.1.2 Power Analysis

The definition of an optimum torsional spring stiffness is when the power required by the motor is minimum. As known, the equation of power is the multiplication of the torque and the velocity. The ankle gait power of humans may be both positive and negative. When it is negative, the ankle is subjected to a resisting motion; when it is positive, the ankle is subjected to a propelling action. Because a motor unit cannot normally generate negative power, it must offer both resistance to and propulsion of human motion. Thus, the formula for the motor power is (Eq. 3.5):

$$P_m = \left|\tau_m \times \dot{\theta}_m\right| \tag{3.5}$$

The calculation of the peak power of the motor was carried out by using Simulink Matlab in an iterative way, where the value of torsional stiffness was defined from 10-1000 Nm/rad. The data of the ankle torque and the ankle position were obtained from the gait study conducted by Winter et al. (1991) – details in Appendix B. the rotational moment of inertia of the ankle value is 0.2 kgm^2 based on studies performed by Rouse et al. (2014), Lee and Hogan (2015) and Shorter and Rouse (2018). As the motor used in this system was Maxon Motor EC-i 52 Ø52 mm, brushless, 200 W, with Hall sensors, the rotational moment of inertia of the motor is 2.64×10^{-6} kgm^2 and the damping coefficient is 2.05×10^{-3} Nms/rad.

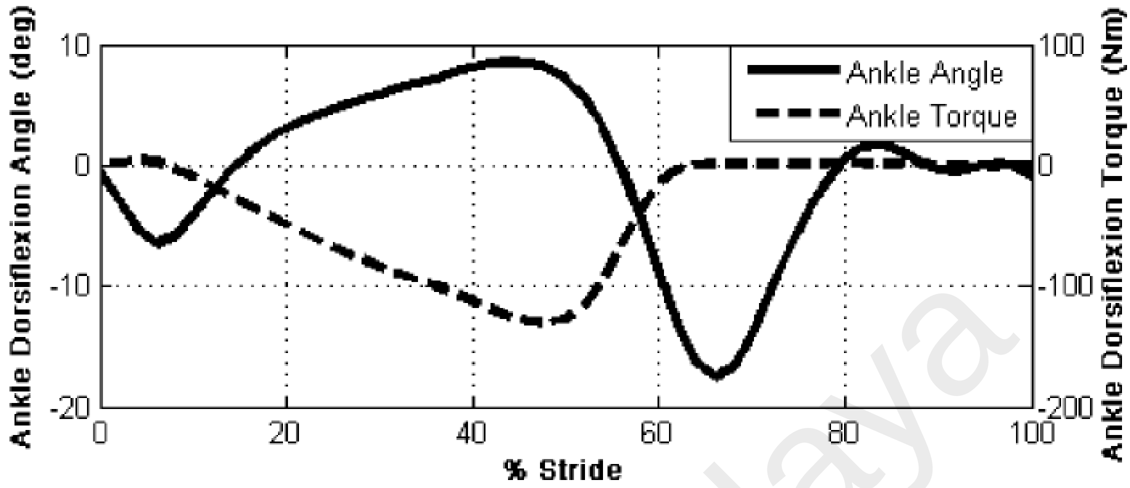

Figure 3.2: Normal biomechanical gait data (adapted from Winter, 1991)

3.2 Topological Shape and Dimension

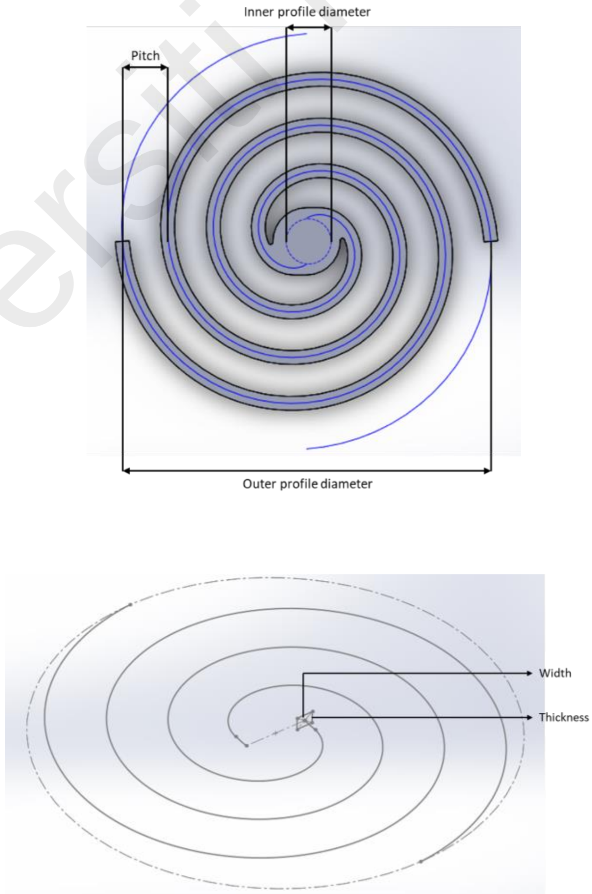

Figure 3.3: The planar rotary spring profile

The spring model was developed by using finite element method in ad hoc way until meet the optimum stiffness value.

Although the spring model was developed in a trial-and-error way, there are some dimension parameters that are assumed to have a fixed value, such as the outer profile diameter of the spring which is 80 mm, the inner profile diameter of the spring which is 10 mm, and the pitch which is 20 mm. The width and thickness of the spring's arm profile were the parameters to be modified until the model reached the optimum stiffness value.

3.3 Finite Element Method

Finite element analysis (FEA) is the technique of modeling the behaviors of a component or assembly under certain constraints and loadings so that it may be examined using the finite element method (FEM). FEA is used by researchers to assist model physical processes and so decrease the requirement for actual prototypes, while allowing for the optimization of components as part of the design phase of a project. In this study, the simulation of finite element analysis was performed in Ansys Workbench 2020.

3.3.1 Material Properties

The material of the spring is Maraging 300 Alloy Steel, which is commercially known as Vascomax-300. Maraging 300 Alloy Steel was selected as it has previously been used for another planar rotary spring model developed by Carpino et al. (2012).

Maraging steels are often machined in the annealed state, although they may be machined in their maraged state as well. Components may be machined near to their final dimensions due to the low temperature maraging treatment. Additionally, the minor contraction caused by maraging (about 0.05%) leads to excellent dimensional stability.

The mechanical properties of the material are presented below (Table 3.1):

Table 3.1: Mechanical properties of Maraging 300 Alloy Steel

Properties	Value
Density	7999.5 kg/m^3
Young's Modulus	1.86 x 10^{11} Pa
Poisson's Ratio	0.3
Tensile Yield Strength	1.91 x 10^9 Pa
Tensile Ultimate Strength	1.96 x 10^9 Pa

3.3.2 Constrains and Loadings

Assisting the definition process of moments operating on the spring, a rigid body was designed and attached to the planar rotary spring model. The material of the rigid body is the same as that of the spring. Furthermore, the rigid body is defined as a contact body and the planar rotary spring is defined as target body.

The fixed support feature defines the inner region of the center hole, as this area is immobile when the moment applies on the spring. Furthermore, the maximum spring torque is defined in the rigid body region. The value of the maximum spring torque can be calculated by using the following equation (Eq. 3.6).

$$\tau_s = \tau_a - J_a\ddot{\theta}_a \tag{3.6}$$

As the value of the rotational moment of inertia of the ankle (J_a) and ankle torque (τ_a) is known. The acceleration of the ankle can be calculated based on the derivation of the ankle position data by Simulink Matlab. The maximum value of the spring torque ($\tau_{s(\max)}$) can be determined as follows:

$$\tau_{s(\max)} = 102.793\ Nm$$

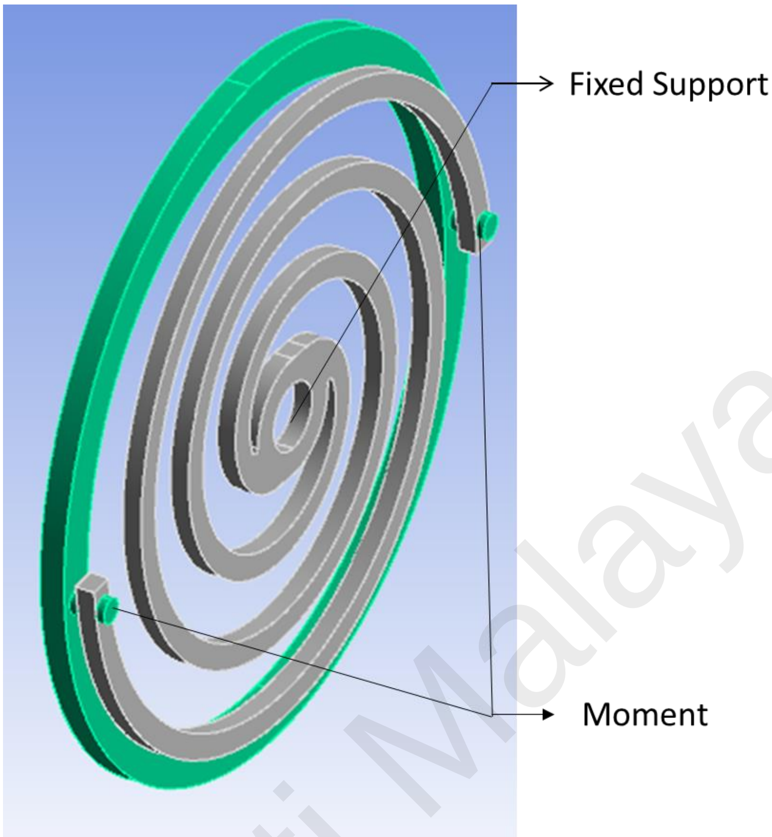

Figure 3.4: Constrains and loadings on the planar rotary spring model

3.3.3 Mesh Model

Meshing is a critical step in generating an accurate FEA simulation. A mesh is composed of components that include nodes (coordinate positions in space that vary according to element type) that define the geometry's form. While the FEA solver is unable to cope with irregular forms, it is considerably more at ease with standard shapes such as cubes. Meshing is the act of transforming amorphous forms into more discernible volumes referred to as "elements." In this mesh model, the element size is $5\text{x}10^{-4}$ m and the meshing method is tetrahedrons.

Figure 3.5: The mesh model of the planar rotary spring

3.3.4 Angular Displacement

The purpose of this simulation is to determine the stiffness of the spring. The spring model can be selected based on the dimension if it has the optimum torsional stiffness value. However, Ansys Workbench does not show stiffness value in the display result. The stiffness value can be obtained with the following equations (Eq. 3.4 and 3.7):

$$\tau_s = -K_s(\theta_m - \theta_a) \tag{3.4}$$

$$\theta_s = \theta_m - \theta_a \tag{3.7}$$

The targeted value of the angular displacement can be obtained if the value of the optimum torsional stiffness of the spring is known, as follows (Eq. 3.8):

$$\theta_s = \frac{\tau_s}{-K_s} \tag{3.8}$$

The APDL command was use to obtain the angular displacement value. In order to use the APDL command, it is necessary to define a remote point in the area where angular displacement is to be investigated (Figure 3.6). The way to execute the APDL command to obtain the angular displacement value is by adding an (APDL)command in the remote point section and writing "Measure_pilot=_npilot," subsequently, create a (APDL)command in the solution section and write "my_rotz=ROTZ (Measure_pilot)." The z-axis was chosen because the spring rotates about the z-axis.

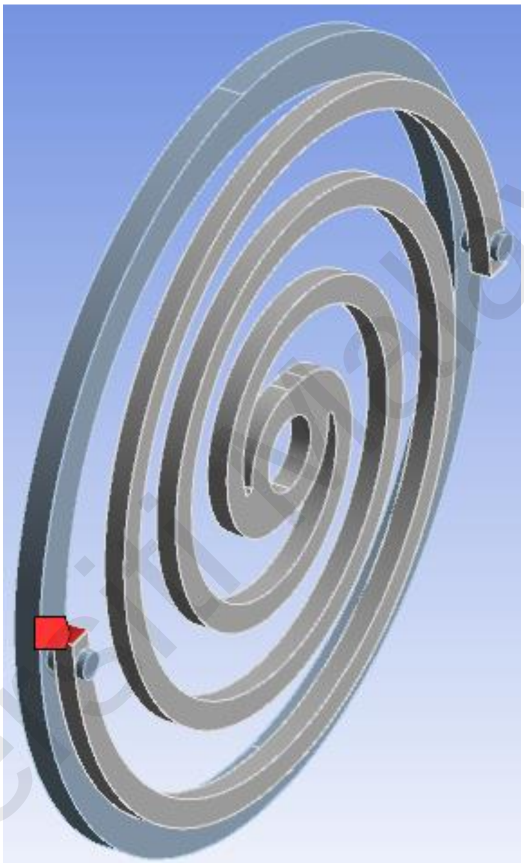

Figure 3.6: The remote point where the angular displacement is probed

CHAPTER 4: RESULT AND DISCUSSION

4.1 The Optimum Torsional Stiffness

By substituting Eq. (3.3) to Eq. (3.1) (see Page 46). The motor torque can be analyzed with the following formula (Eq. 4.1):

$$\tau_m = J_m \ddot{\theta}_m + B_m \dot{\theta}_m + K_s \theta_m - K_s \theta_a \tag{4.1}$$

The position of the motor can be obtained by substituting Eq. (3.4) to Eq. (3.2), as follows (Eq. 4.2):

$$\theta_m = \frac{1}{K_s} J_a \ddot{\theta}_a + \theta_a - \frac{1}{K_s} \tau_a \tag{4.2}$$

As the equation will be solved by using Matlab Simulink, the motor position can be determined by its derivation.i.e. (Eq. 4.3 and 4.4):

$$\dot{\theta}_m = \frac{1}{K_s} \dot{J}_a \dddot{\theta}_a + \dot{\theta}_a - \frac{1}{K_s} \dot{\tau}_a \tag{4.3}$$

$$\ddot{\theta}_m = \frac{1}{K_s} \ddot{J}_a \ddddot{\theta}_a + \ddot{\theta}_a - \frac{1}{K_s} \ddot{\tau}_a \tag{4.4}$$

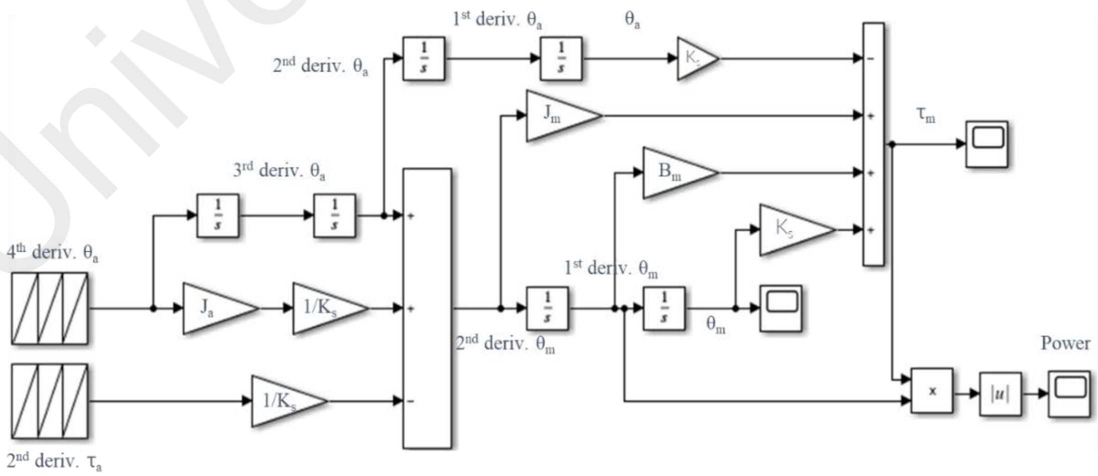

Figure 4.1: Block diagram of the rotary SEA's dynamic model

From the calculation of peak power of the motor by using Matlab Simulink, the optimum torsional stiffness of the motor was in between 620-630 Nm/rad – detail in Appendix A – with the peak power of 115.600 Watt. Based on the data, the time for one full gait cycle was 1.13 seconds. The minimum peak power of the motor is occurred at 0.543 seconds or 48.05% of the gait cycle when the stiffness was 620 Nm/rad an 0.545 or 48.23% when the stiffness was 630 Nm/rad.

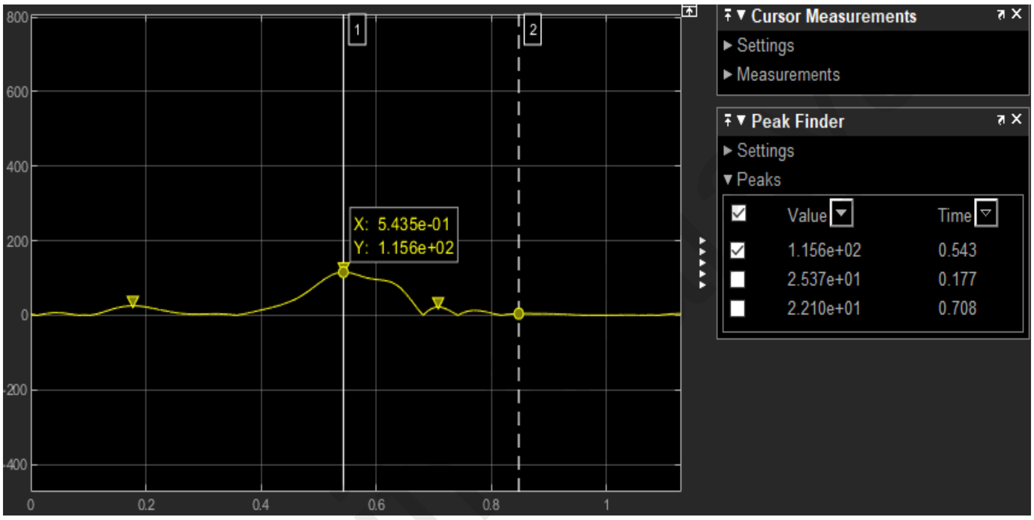

Figure 4.2: Display result of the peak power when the torsional stifness is 620 Nm/rad by using Matlab Simulink

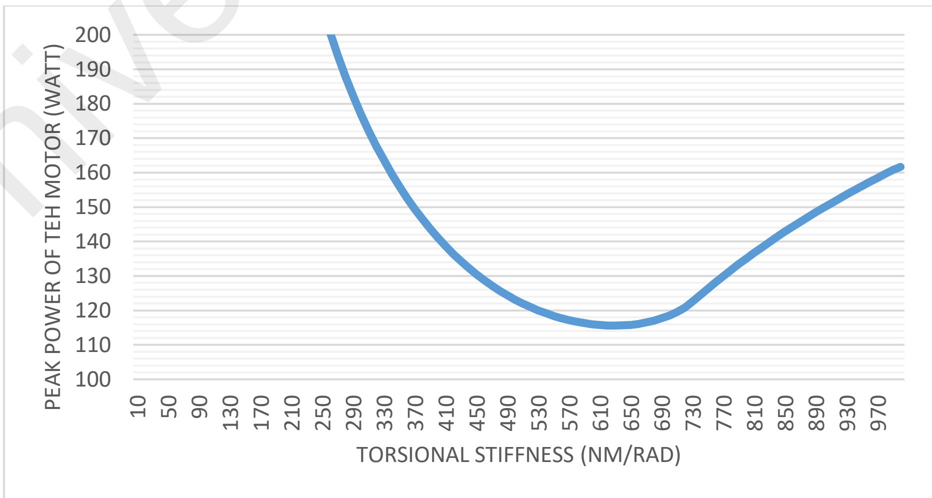

Figure 4.3: Chart of power peak of the motor with torsional stiffness 10 to 1000 Nm/rad

It has also been demonstrated in (Paluska & Herr, 2006) that the adequate selection of spring stiffness for a certain application can lead to an energetic optimization of the system. The main disadvantage introduced by the series elastic element is a reduction in actuator bandwidth (Hurst, et al., 2004): a higher compliance of the actuator reduces the torque control's bandwidth. As a direct result of this behavior, given a target torque control parameter, a SEA may require more power than a standard stiff motor. Furthermore, when the system is stiffness-controlled (that is, it emulates elastic behavior) and conservative stability restrictions must be met, the highest stiffness that may be displayed is restricted to the physical stiffness of the elastic element (Vallery, et al., 2008).

Figure 4.3 shows an intriguing relationship. At stiffness values close to zero, limitless motor power is required. It can be seen that a high stiffness spring approaches maximal gait power asymptotically near 160 W. Instead of a linear relationship between the two extremes, a minimum point or cusp occurs. A 1/K relationship with respect to power determines the driving profile for this plot. The cusp is created as a function of the absolute value of this factor and hence a minimum is created.

4.2 Finite Element Analysis Results

The targeted angular displacement can be calculated as the value of the maximum spring torque and the optimum torsional stiffness are known, with the following formula (Eq. 4.5).

$$\theta_s = \left|\frac{\tau_s}{-K_s}\right| \tag{4.5}$$

$$\theta_s = \left|\frac{102.793\ Nm}{-620\ Nm/rad}\right| \text{ and } \theta_s = \left|\frac{102.793\ Nm}{-630\ Nm/rad}\right|$$

$$\theta_s = \ in\ between\ 0.163 \text{ rad and } 0.165 \text{ rad}$$

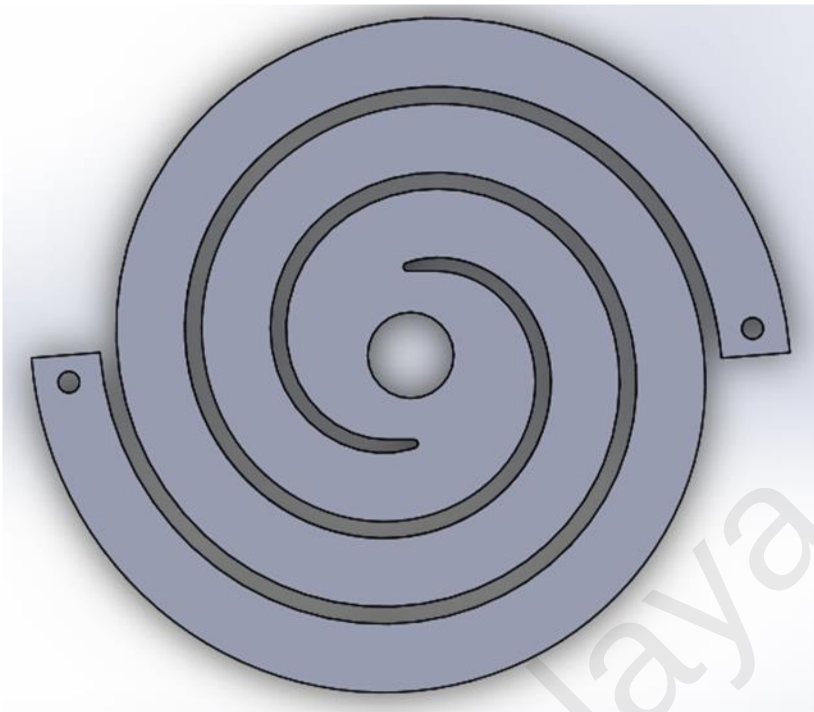

Figure 4.4: The planar rotary spring for the BioApps RoMicP® ankle-foot prosthesis

Based on the APDL command the angular displacement of the planar rotary spring for the BioApps RoMicP® ankle-foot prosthesis (with the width and the thickness dimensions are 7.95 mm and 8 mm consecutively) was 0.163 rad. The mass of the planar rotary spring model was 0.256 kg. Other SEA designs have maximum spring deflections that range from ±0.052 rad to ±0.872 rad (Tsagarakis et al., 2009; Kong et al., 2012; (Cummings et al., 2016).

In Figure 4.2 and 4.3, elastic module deformation and Von-Mises stress as obtained by the FEM simulation were reported under an applied torque of 102.793 Nm. The deformation of the spring was 0.007 meter. The maximum resultant Von-Mises stress was 1.40 x 109 Pa. Considering that the yield stress of the selected material was 1.91 x 109 Pa, a safety factor of 1.36 was achieved.

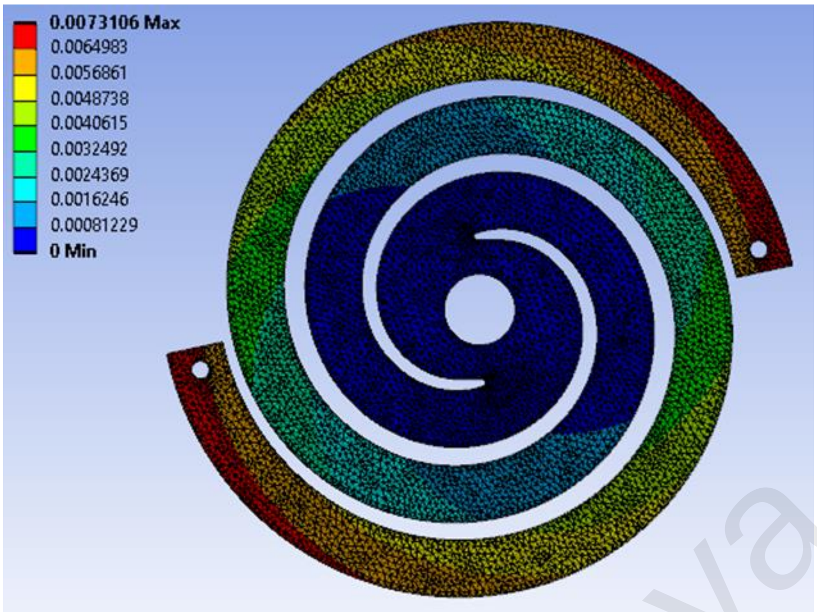

Figure 4.5: The deformation (in meter) of the planar rotary spring

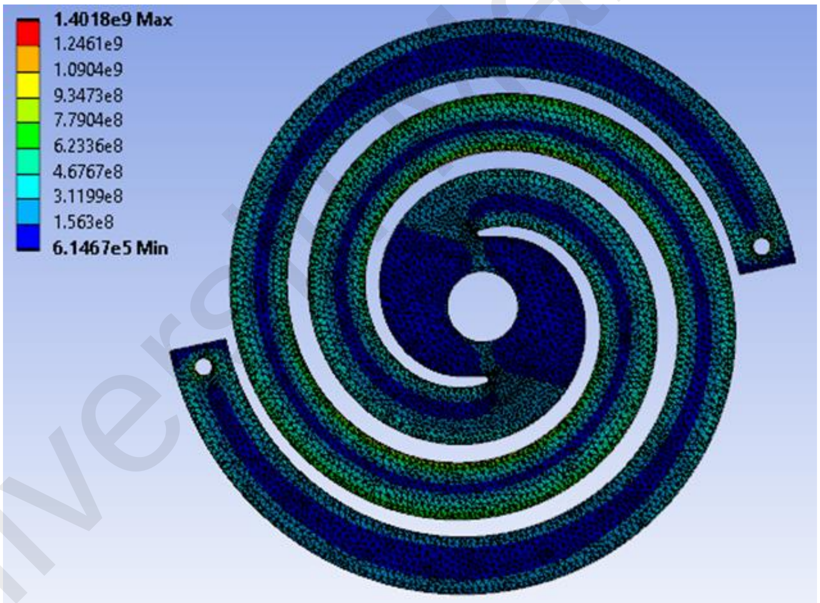

Figure 4.6: The Von-Mises stress (in pascal) of the planar rotary spring

CHAPTER 5: CONCLUSION AND FUTURE WORK

5.1 Conclusion

In this research project the preliminary design of planar rotary as one of the major components of the SEA system in BioApps RoMicP® ankle-foot prosthesis is presented. The spring was developed by iterative shape optimization using Finite Element Analysis (FEA). This research has answered three main objectives described in Chapter 1.

The first objective described in this project was to calculate the required stiffness of planar rotary spring according to the requirement of powered ankle-foot prosthesis. The definition of an optimum torsional spring stiffness is when the power required by the motor is minimum. From the calculation of peak power of the motor by using Matlab Simulink, the optimum torsional stiffness of the motor was in between 620-630 Nm/rad

The second objective was to model an effective design with appropriate material and topological shape. Archimedean spiral was chosen as the topological shape of the spring. The spring model was developed by using finite element method in ad hoc way until meet the optimum stiffness value. The material of the spring used was Maraging 300 Alloy Steel, commercially known as Vascomax-300.

The final objective was to simulate the stiffness of spring via the method of Finite Element Analysis (FEA) to verify the design. The width and thickness of the spring's arm profile were the parameters to be modified until the model reached the optimum stiffness value. Based on the simulation result, the optimum torsional stiffness was reached when the width and the thickness of the planar rotary spring's arm profile are 8 mm and 7.95 consecutively. Furthermore, the planar rotary spring model was able to withstand a maximum torque of 102.793 Nm.

5.2 Future Work

The preliminary design of a planar rotary spring for BioApps RoMicP® ankle-foot prosthesis was achieved as an outcome of this study. For forthcoming works, the prototype of the spring design can be manufactured to determine if the design can be successfully applied to a rotary series elastic actuator system.

Furthermore, this novel design opens up an entire design space with potential optimization and performance trade-offs that fixed. The main advantage of the presented spring design is the ability to undergo comparatively lower peak power of the motor, and this thesis provides the fundamentals required to further parametrize and optimize the torsion spring design for specific applications.

The optimization of the preliminary design can be performed, for instance, reducing the mass of the planar rotary spring by performing cutouts as introduced by Georgiev and Burdick (2017).

REFERENCES

Alamdari, A., and Krovi, V. N. (2017). A Review of Computational Musculoskeletal Analysis of Human Lower Extremities. Human Modelling for Bio-Inspired Robotics, 37–73. https://doi.org/10.1016/b978-0-12-803137-7.00003-3

Arifin, N., Hasbollah, H. R., Hanafi, M. H., Ibrahim, A. H., Wan Abdul Rahman, W. A., and Che Aziz, R. (2017). Provision of Prosthetic Services Following Lower Limb Amputation in Malaysia. Malaysian Journal of Medical Sciences, 24(5), 106–111. https://doi.org/10.21315/mjms2017.24.5.12

Au, S., Weber, J., and Herr, H. (2009). Powered Ankle–foot Prosthesis Improves Walking Metabolic Economy. IEEE Transactions on Robotics, 25(1):51–66.

Baker, R. (2006). Gait Analysis Methods in Rehabilitation. Journal of NeuroEngineering and Rehabilitation, 3(1). https://doi.org/10.1186/1743-0003-3-4

Bellman, R. D., Holgate, M. A., and Sugar, T. G. (2008). Sparky 3: Design of an Active Robotic Ankle Prosthesis with Two Actuated Degrees of freedom Using Regenerative Kinetics. In 2nd IEEE RAS & EMBS International Conference on Biomedical Robotics and Biomechatronics (BioRob), Scottsdale, pages 511–516. IEEE.

Bertomeu-Motos, A. (2016). Biomechanics of Human Walking and Stability Descriptive Parameters. Revista Doctorado UMH, 2(1), 4. https://doi.org/10.21134/doctumh.v1i1.880

Carpino, G., Accoto, D., Sergi, F., Luigi Tagliamonte, N., and Guglielmelli, E. (2012). A Novel Compact Torsional Spring for Series Elastic Actuators for Assistive Wearable Robots. Journal of Mechanical Design, 134(12). https://doi.org/10.1115/1.4007695

Cherelle, P., Matthys, A., Grosu, V., Brackx, B., Van Damme, M., Vanderborght, B., and Lefeber, D. (2012). The AMP-foot 2.0: A Powered Transtibial Prosthesis that Mimics Intact Ankle Behavior. In 9th National Congress on Theoretical and Applied Mechanics, Brussels.

Colborne, G. R., Naumann, S., Longmuir, P. E., and Berbrayer, D. (1992). Analysis of Mechanical and Metabolic Factors in The Gait of Congenital Below Knee Amputees. American Journal of Physical Medicine & Rehabilitation, 71(5), 272–278. https://doi.org/10.1097/00002060-199210000-00004

Cummings, J. P., Ruiken, D., Wilkinson, E. L., Lanighan, M. W., Grupen, R. A., and Sup, F. C. (2016). A Compact, Modular Series Elastic Actuator. Journal of Mechanisms and Robotics, 8(4). https://doi.org/10.1115/1.4032975

Dillingham, T. R., Pezzin, L. E., and Mackenzie, E. J. (2002). Limb Amputation and Limb Deficiency: Epidemiology and Recent Trends in the United States. Southern Medical Journal, 95(8), 875–883. https://doi.org/10.1097/00007611-200208000-00018

Donatelli, R. (1985). Normal Biomechanics of the Foot and Ankle. Journal of Orthopaedic & Sports Physical Therapy, 7(3), 91–95. https://doi.org/10.2519/jospt.1985.7.3.91

EC-I 52 ø52 mm, brushless, 200 W, with Hall Sensors: High torque. Online shop for high Precise Drive Systems by Maxon | Maxon Group. (n.d.). Retrieved January 13, 2022, from https://www.maxongroup.com/maxon/view/product/606793

Ehara, Y., Beppu, M., Nomura, S., Kunimi, Y., and Takahashi, S. (1993). Energy Storing Property of So-called Energy-Storing Prosthetic Feet. Archives of physical medicine and rehabilitation, 74(1), 68–72.

Eilenberg, M., Geyer, H., and Herr, H. (2010). Control of a Powered Ankle–foot Prosthesis Based on a Neuromuscular Model. IEEE Transactions on Neural Systems and Rehabilitation Engineering, 18(2):164–173.

Englsberger, J., Werner, A., Ott, C., Henze, B., Roa, M. A., Garofalo, G., Burger, R., Beyer, A., Eiberger, O., Schmid, K., and et al. (2014). Overview of the Torque-controlled Humanoid Robot TORO. 2014 IEEE-RAS International Conference on Humanoid Robots.

Eslamy, M., Grimmer, M., Rinderknecht, S., and Seyfarth, A. (2013). Does It Pay to Have a Damper in a Powered Ankle Prosthesis? a power-energy Perspective. In IEEE International Conference on Rehabilitation Robotics (ICORR).

Eslamy, M., Grimmer, M., and Seyfarth, A. (2012). Effects of Unidirectional Parallel Springs on Required Peak Power and Energy in Powered Prosthetic Ankles: Comparison Between Different Active Actuation Concepts. In IEEE International Conference on Robotics and Biomimetics (ROBIO).

Ferris, D. P., Czerniecki, J. M., Hannaford, B., and et al. (2005). An Ankle-foot Orthosis Powered by Artificial Pneumatic Muscles. Journal of Applied Biomechanics, 21(2):189.

Fradet, L., Alimusaj, M., Braatz, F., and Wolf, S. I. (2010). Biomechanical Analysis of Ramp Ambulation of Transtibial Amputees with An Adaptive Ankle Foot System. Gait & Posture, 32(2):191–198.

Gailey, R., Allen, K., Castles, J., Kucharik, J., and Roeder, M. (2008). Review of Secondary Physical Conditions Associated with Lower-limb Amputation and Long-term Prosthesis Use. Journal of Rehabilitation Research and Development, 45(1):15.

Geeroms, J. (2011). Study and Design of an Actuated Below-knee Prosthesis (thesis).

Georgiev, N., and Burdick, J. (2017). Design and Analysis of Planar Rotary Springs. 2017 IEEE/RSJ International Conference on Intelligent Robots and Systems (IROS). https://doi.org/10.1109/iros.2017.8206352

Grimmer, M., Eslamy, M., Gliech, S., and Seyfarth, A. (2012). A Comparison of Parallel and Series Elastic Elements in An Actuator for Mimicking Human Ankle Joint In

Walking And Running. In IEEE International Conference on Robotics and Automation (ICRA), St. Paul, pages 2463–2470. IEEE.

Grimmer, M. and Seyfarth, A. (2011a). Stiffness Adjustment of a Series Elastic Actuator in a Knee Prosthesis for Walking And Running: The Trade-off Between Energy and Peak Power Optimization. In IEEE/RSJ International Conference on Intelligent Robots and Systems (IROS), San Francisco, pages 1811–1816. IEEE.

Grimmer, M. and Seyfarth, A. (2011b). Stiffness Adjustment of a Series Elastic Actuator in an Ankle-foot Prosthesis for Walking And Running: The Trade-off between Energy and Peak Power Optimization. In IEEE International Conference on Robotics and Automation (ICRA), Shanghai, pages 1439–1444. IEEE.

Hall, S. J. (2012). Basic Biomechanics. McGraw-Hill.

Herr, H. M., Au, S. K., Dilworth, P., and Paluska, D. J. (2012). Artificial Ankle-Foot System with Spring, Variable-damping, And Series Elastic Actuator Components. US Patent App. 13/348,570.

Hitt, J., Merlo, J., Johnston, J., Holgate, M., Boehler, A., Hollander, K., and Sugar, T. (2010a). Bionic Running for Unilateral Transtibial Military Amputees. Technical report, DTIC Document.

Hitt, J., Sugar, T., Holgate, M., and Bellman, R. (2010b). An Active Foot-ankle Prosthesis with Biomechanical Energy Regeneration. Journal of Medical Devices, 4:011003.

Hobbelen, D., Boer, T. D., and Wisse, M. (2008). System Overview of Bipedal Robots Flame and Tulip: Tailor-made for Limit Cycle Walking. 2008 IEEE/RSJ International Conference on Intelligent Robots and Systems.

Hollander, K. and Sugar, T. (2005). Design of the Robotic Tendon. In Design of Medical Devices Conference (DMD).

Hurst, J. and Green, K. (2020). Series Elastic Actuation. Encyclopedia of Robotics, pp. 1–12.

Hurst, J., Rizzi, A., and Hobbelen, D. (2004). Series elastic actuation: Potential and pitfalls. International Conference on Climbing and Walking Robots.

Kim, J., Lee, Y., Kwon, S., Seo, K., Kwak, H., Lee, H., and Roh, K. (2012). Development of the Lower Limbs for a Humanoid Robot. IEEE/RSJ International Conference on Intelligent Robots and Systems.

Knabe, C., Lee, B., Orekhov, V., and Hong, D. (2014). Design of a Compact, Lightweight, Electromechanical Linear Series Elastic Actuator. Volume 5B: 38th Mechanisms and Robotics Conference.

Knox, B. T., and Schmiedeler, J. P. (2009). A Unidirectional Series Elastic Actuators Design Using a Spiral Torsion Spring. Journal of Mechanical Design, VOL. 131.

Kong, K., Bae, J., and Tomizuka, M. (2012). A Compact Rotary Series Elastic Actuator for Human Assistive Systems. IEEE/ASME Transactions on Mechatronics, 17(2), 288–297. https://doi.org/10.1109/tmech.2010.2100046

Lagoda, C., Schouten, A. C., Stienen, A. H., Hekman, E. E., and van der Kooij, H. (2010). Design of an Electric Series Elastic Actuated Joint for Robotic Gait Rehabilitation Training. 2010 3rd IEEE RAS & EMBS International Conference on Biomedical Robotics and Biomechatronics. https://doi.org/10.1109/biorob.2010.5626010

Lee, B., Knabe, C., Orekhov, V., and Hong, D. (2014). Design of a Human-like Range of Motion Hip Joint for Humanoid Robots. Volume 5B: 38th Mechanisms and Robotics Conference.

Lee, H., and Hogan, N. (2015). Time-Varying Ankle Mechanical Impedance During Human Locomotion. IEEE Transactions on Neural Systems and Rehabilitation Engineering, 23(5), 755–764. https://doi.org/10.1109/tnsre.2014.2346927

Liu, J., Abu Osman, N. A., Al Kouzbary, M., Al Kouzbary, H., Abd Razak, N. A., Shasmin, H. N., and Arifin, N. (2021). Classification and Comparison of Mechanical Design of Powered Ankle–foot Prostheses for Transtibial Amputees Developed in the 21st Century: A Systematic Review. Journal of Medical Devices, 15(1). https://doi.org/10.1115/1.4049437

Lusardi, M., Jorge, M., and Nielsen, C. (2013). Orthotics and Prosthetics in Rehabilitation (3rd ed.). Elsevier Saunders.

Michael, J.M., Golshani, A., Gargac, S., and Goswami, T. (2008). Biomechanics of the Ankle Joint and Clinical Outcomes of Total Ankle Replacement. J Mech Behav Biomed Mater. 1(4): p. 276-94

Molen, N. H. (1973). Energy/Speed Relation of Below-knee Amputees Walking on a Motor-driven Treadmill. Internationale Zeitschrift für Angewandte Physiologie Einschliesslich Arbeitsphysiologie, 31(3), 173–185. https://doi.org/10.1007/bf00697597

Molina C.S., Faulk J.B. (2021). Lower Extremity Amputation. StatPearls Publishing. Available from: https://www.ncbi.nlm.nih.gov/books/NBK546594/

Moxey, P. W., Gogalniceanu, P., Hinchliffe, R. J., Loftus, I. M., Jones, K. J., Thompson, M. M., and Holt, P. J. (2011). Lower Extremity Amputations - A Review of Global Variability in Incidence. Diabetic Medicine, 28(10), 1144–1153. https://doi.org/10.1111/j.1464-5491.2011.03279.x .

Negrello, F., Garabini, M., Catalano, M. G., Malzahn, J., Caldwell, D. G., Bicchi, A., and Tsagarakis, N. G. (2015). A Modular Compliant Actuator for Emerging High Performance and Fall-resilient Humanoids. IEEERAS 15th International Conference on Humanoid Robots (Humanoids).

Nigg, B. M., Herzog, W., and Herzog, W. (1994). Biomechanics of the Musculo-skeletal System. Wiley New York.

Orekhov, V. L., Knabe, C. S., Hopkins, M. A., and Hong, D. W. (2015). An Unlumped Model for Linear Series Elastic Actuators with Ball Screw Drives. 2015 IEEE/RSJ International Conference on Intelligent Robots and Systems (IROS).

Orekhov, V.L., Lahr, D., Lee, B., and Hong, D. (2013). Configurable Compliance for Series Elastic Actuators. Volume 6B: 37th Mechanisms and Robotics Conference.

Pierrynowski, M. R. and Morrison, J. B. (1985). A Physiological Model for the Evaluation of Muscular Forces in Human Locomotion: Theoretical Aspects. Mathematical Biosciences, 75(1):69– 101.

Popovic, D., Tomovic, R., Tepavac, D., and Schwirtlich, L. (1991). Control Aspects of Active Above-knee Prosthesis. International Journal of Man-Machine Studies, 35(6):751–767.

Robbins, C., Vreeman, D., Sothmann, M., Wilson, S., and Oldridge, N. (2009). A Review of The Long-term Health Outcomes Associated with War-related Amputation. Military Medicine, 174(6):588–592.

Robinson, D.W. (2000). Design And Analysis of Series Elasticity in Closed-loop Actuator Force Control. PhD thesis, Massachusetts Institute of Technology, Cambridge, MA.

Rodrigues, D. S. de O. S. (2013). Biomechanics of the Total Ankle Arthroplasty: Stress Analysis and Bone Remodeling (thesis).

Rouse, E. J., Hargrove, L. J., Perreault, E. J., and Kuiken, T. A. (2014). Estimation of Human Ankle Impedance During the Stance Phase of Walking. IEEE Transactions on Neural Systems and Rehabilitation Engineering, 22(4), 870–878. https://doi.org/10.1109/tnsre.2014.2307256

Paine, N., Mehling, J. S., Holley, J., Radford, N. A., Johnson, G., Fok, C.-L., and Sentis, L., (2015). Actuator Control for the NASA-JSC Valkyrie Humanoid Robot: A Decoupled Dynamics Approach for Torque Control of Series Elastic Robots. Journal of Field Robotics, 32(3), p. 378396.

Paine, N., Oh, S., and Sentis, L. (2014). Design and Control Considerations for High Performance Series Elastic Actuators. IEEE/ASME Transactions on Mechatronics, 19(3), p. 10801091.

Pedotti A. (1977) Simple Equipment Used in Clinical Practice for the Evaluation of Locomotion. IEEE Transactions on Biomedical Engineering BME-24: 456–461.

Perry, J. and Burnfield, J. (1992) Gait Analysis: Normal and Pathological Function. SLACK Incorporated, New Jersey.

Pratt, G. A. and Williamson, M. M. (1995). Series Elastic Actuators. IEEE/RSJ International Conference on Intelligent Robots and Systems. Human Robot Interaction and Cooperative Robots.

Pratt, J., and Krupp, B. (2008). Design of a Bipedal Walking Robot. Unmanned Systems Technology X.

Pratt, J., Krupp, B., and Morse, C. (2002). Series Elastic Actuators for High Fidelity Force Control. Industrial Robot: An International Journal, 29(3), p. 234241.

Paluska, D., and Herr, H. (2006). The effect of series elasticity on actuator power and work output: Implications for robotic and Prosthetic Joint Design. Robotics and Autonomous Systems, 54(8), 667–673. https://doi.org/10.1016/j.robot.2006.02.013

Sammarco G.J., Hockenbury R.T. (2001). Biomechanics of the Foot and Ankle. In: Nordin M, Frankel VH, eds. Basic Biomechanics of the Musculoskeletal System (3rd ed). Philadelphia: Lippincott Williams & Wilkins, pp. 222-255

Sawicki, G. S. and Ferris, D. P. (2009). A Pneumatically Powered Knee-ankle-Foot Orthosis (KAFO) With Myoelectric Activation and Inhibition. Journal of Neuroengineering and Rehabilitation, 6(1):23.

Schinder, A., Genao, C., and Semmelroth, S. (2011). Methodology for Control and Analysis of an Active Foot-ankle Prosthesis. Proceedings of The National Conference on Undergraduate Research (NCUR) 2011 Ithaca College, New York, pages 2011 –2018.

Schumacher, S.A. (2012). Achilles Foot Health Centre. Available from: http://www.footdoc.ca/www.FootDoc.ca/Website%20Definitions%20(Basic%20 Terms).htm.

Shorter, A. L., and Rouse, E. J. (2018). Mechanical Impedance of the Ankle During the Terminal Stance Phase of Walking. IEEE Transactions on Neural Systems and Rehabilitation Engineering, 26(1), 135–143. https://doi.org/10.1109/tnsre.2017.2758325

Stienen, A. H. A. (2009). Development of Novel Devices for Upperextremity Rehabilitation. PhD thesis, University of Twente, Twente, The Netherlands.

Stienen, A. H. A., Hekman, E. E. G., ter Braak, H., Aalsma, A. M. M., van der Helm, F. C. T., and van der Kooij, H. (2010). Design of a Rotational Hydroelastic Actuator for a Powered Exoskeleton for Upper Limb Rehabilitation. IEEE Transactions on Biomedical Engineering, 57(3), 728–735. https://doi.org/10.1109/tbme.2009.2018628

Sun, X., Sugai, F., Okada, K., and Inaba, M. (2018). Design, Control and Preliminary Test of Robotic Ankle Prosthesis. 2018 IEEE/RSJ International Conference on Intelligent Robots and Systems (IROS). https://doi.org/10.1109/iros.2018.8594498

Sup, F., Varol, H., Mitchell, J., Withrow, T., and Goldfarb, M. (2009). Self-contained Powered Knee and Ankle Prosthesis: Initial Evaluation on a Transfemoral Amputee. In IEEE International Conference on Rehabilitation Robotics (ICORR), Kyoto, pages 638–644. IEEE.

Svensson, W. and Holmberg, U. (2006). An Autonomous Control System for a Prosthetic Foot Ankle. In 4th IFAC Symposium on Mechatronic Systems (2006), pages 856–861. International Federation of Automatic Control (IFAC).

Tsagarakis, N. G., Laffranchi, M., Vanderborght, B., and Caldwell, D. G. (2009). A compact soft actuator unit for small scale Human Friendly Robots. 2009 IEEE International Conference on Robotics and Automation. https://doi.org/10.1109/robot.2009.5152496

Tsagarakis, N. G., Morfey, S., Cerda, G. M., Zhibin, L., and Caldwell, D. G. (2013). COMpliant huMANoid COMAN: Optimal Joint Stiffness Tuning for Modal Frequency Control. 2013 IEEE International Conference on Robotics and Automation.

Vallery, H., Veneman, J., van Asseldonk, E., Ekkelenkamp, R., Buss, M., and van der Kooij, H. (2008). Compliant actuation of rehabilitation robots: benefits and limitations of series elastic actuators. IEEE Robotics & Automation Magazine, 15(3), pp. 60–69.

van Oort, G., Carloni, R., Borgerink, D. J., and Stramigioli, S. (2011). An Energy Efficient Knee Locking Mechanism for a Dynamically Walking Robot. 2011 IEEE International Conference on Robotics and Automation. https://doi.org/10.1109/icra.2011.5980276

Versluys, R., Lenaerts, G., Van Damme, M., Jonkers, I., Desomer, A., Vanderborght, B., Peeraer, L., Van der Perre, G., and Lefeber, D. (2009). Successful Preliminary Walking Experiments on a Transtibial Amputee Fitted with a Powered Prosthesis. Prosthetics and Orthotics International, 33(4):368–377.

Wang, S., van Dijk, W., and van der Kooij, H. (2011). Spring Uses in Exoskeleton Actuation Design. In IEEE International Conference on Rehabilitation Robotics (ICORR), pages 1–6. IEEE.

Windrich, M., Grimmer, M., Christ, O., Rinderknecht, S., and Beckerle, P. (2016). Active Lower Limb Prosthetics: A Systematic Review of Design Issues and Solutions. BioMedical Engineering OnLine, 15(S3). https://doi.org/10.1186/s12938-016-0284-9

Winter, D. (1991). The Biomechanics and Motor Control of Human Gait: Normal, Elderly and Pathological, 2nd ed. Waterloo, Univ. Waterloo Press.

Winter, D. A., and Sienko, S. E. (1988). Biomechanics of Below-knee Amputee Gait. Journal of Biomechanics, 21(5), 361–367. https://doi.org/10.1016/0021-9290(88)90142-x

Whittle, M. W. (2002). Gait Analysis: An Introduction (3rd Edition). Elsevier.

World Health Organization (2011). World Report on Disability. Retrieved from https://apps.who.int/iris/rest/bitstreams/53067/retrieve

Yuan, K., Zhu, J., Wang, Q., and Wang, L. (2011). Finite-state Control of Powered Below-knee Prosthesis with Ankle and Toe. In Proc. 18th IFAC World Congress, pages 2865–2870.

Zajac, F. E. et al. (1989). Muscle and Tendon: Properties, Models, Scaling, and Application to Biomechanics and Motor Control. Critical Reviews in Biomedical Engineering, 17(4):359.

Zhu, J., Wang, Q., and Wang, L. (2010). Pantoe 1: Biomechanical Design of Powered Ankle-foot Prosthesis with Compliant Joints and Segmented Foot. In IEEE/ASME International Conference on Advanced Intelligent Mechatronics (AIM), pages 31–36. IEEE.